Journal of Materials Chemistry A

Accepted Manuscript

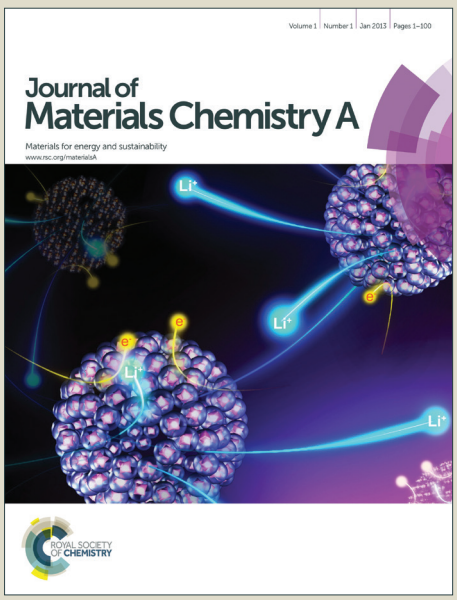

ROYAL SOCIETY OF CHEMISTRY

www.rsc.org/materialsA

Solid-State Gas Sensors for High Temperature Application – A Review

Yixin Liu*, Joseph Parisi, Xiangcheng Sun, Yu Lei*

Department of Chemical and Biomolecular Engineering
University of Connecticut
191 Auditorium Road, Unit 3222,
Storrs, Connecticut 06269
USA

* To whom correspondence should be addressed:
Email: yil10003@engr.uconn.edu; ylei@engr.uconn.edu
Tel: 1-860-486-4554
Fax: 1-860-486-2959

Abstract:

The development of high temperature gas sensors for industrial applications such as combustion process is essential to improve the energy efficiency and reduce toxic emissions. However, gas sensors operated at high temperature up to 1000 ^{o}C, typically encounter many challenging issues, such as thermal and long-term stability, sensitivity, reproducibility and selectivity. This review article discusses various solid-state gas sensors which can be operated at high temperature above 600 ^{o}C. Basic working principles for each type of solid-state gas sensors are briefly introduced, including potentiometric, amperometric, resistive and impedancemetric sensors. Key results and discussion of previous studies on high temperature O_2, CO, HCs and NO_x sensors are also presented with emphasis on the development of suitable electrolytes and sensing materials with good thermal stability and sensing performance for such high temperature gas sensing application. The challenges and scope for future development were finally discussed.

Keywords: high temperature; gas sensors; solid-state gas sensors; review

Contents:

1. Introduction

The recent rapid development in science and technology has produced a remarkable rise in our living standards. However, along with these great developments, a variety of environmental problems have been created which have increased worldwide environmental concerns. Since the gaseous pollutants released from industries and automobiles can diffuse rapidly over large areas within a short period of time, the resulted atmospheric pollution has created major concerns such as human health issues, acid rain, ozone depletion and the greenhouse effect.[1] The combustion of fossil fuels is a major source of air pollution which has been under increased scrutiny by public and government organizations.[2] Besides the environmental and health concerns, there is also a rapid depletion of various energy sources, which forces energy saving to become a major global focus. Gas sensors analyzing composition of emission gases allow the combustion process to be optimized by adjusting the control parameters (e.g., fuel/air stoichiometry and combustion temperature) via a feedback control system, thus resulting in reduced emissions, improved energy efficiency and lower operating costs. Industries such as power generation, automotive, aerospace, glass, ceramic, petrochemical and food-processing industries which are heavily associated with combustion process, require the sensors to work in harsh environments (e.g., high temperature, high pressure, corrosive environment, high spatial velocity of exhausts, etc.). According to a U.S. Department of Energy report, harsh environment sensors if successfully employed are predicted to save 0.25 quadrillion BTU/year of energy across all energy-consuming industries. [3]

High temperature gas sensors, as the most common type of sensors working in harsh environment, play an important role in the monitoring and control of combustion process. While the monitoring of the oxygen content is the primary method to optimize the combustion process, emission control also requires the monitoring of carbon monoxide (CO), hydrocarbons (HCs) and nitrogen oxides (NO_x). Take the automotive engines as an example, Table 1 reports typical compositions of exhaust gases for some common engine types. [4] The exhaust contains three primary pollutants - unburned or partially burned hydrocarbons (HCs), CO and NO_x (mostly NO). Also, the exhaust gases in close proximity to the engine can reach up to 1000 ^oC. In order to achieve the *in-situ* monitoring of combustion gas components at high temperature for optimization, the gas compositions need to be determined directly in the high temperature environment, which is a challenge for many sensing technologies.

Current sensing technologies based on calorimetry, chromatography, and spectroscopic techniques are either too expensive or cumbersome for *in-situ* measurements in industrial environments involving high temperature and chemical contaminants. Among various approaches used, solid-state gas sensing technology is particularly well suited to high temperature aggressive environments due to its high thermal stability compared to other technologies. Other advantages of solid-state high temperature gas sensors include a low cost, simple structure, ease of fabrication and compatibility with electronic systems. [3] Therefore, there is an urgent demand to develop miniaturized, robust and cost-effective high temperature gas sensors with good thermal stability, high sensitivity and selectivity.

[Table 1]

In the past three decades, various solid-state sensors have been developed for monitoring combustion processes at high temperature.[5, 6] However, analysis of a sample gas at lower temperatures is more widely used in industrial practice due to the lack of durable and reliable high temperature gas sensors. This review aims at summarizing solid-state high temperature gas sensors which can be operated above 600 ^{o}C and emphasizes on the development of suitable electrolytes and sensing materials with good thermal stability and sensing performance. Starting with a brief introduction of the working principles of different solid-state gas sensing technologies, this review will then discuss the progress of various high temperature gas sensors for O_2, CO, HCs and NO_x, and finally closed with the challenges that they are facing in high temperature applications and future trends.

2. Solid State Gas Sensing Technologies

Based on sensing principles and sensor configurations, gas sensors can be classified in three categories: (i) solid electrolyte-based gas sensors (potentiometric and amperometric gas sensors), (ii) resistive gas sensors based on semiconducting metal oxides and (iii) impedancemetric gas sensors which employs AC measurements and can be operated in both solid electrolyte-based and semiconductor-based configurations.

2.1 Solid electrolyte-based gas sensors

Potentiometric and amperometric gas sensors belong to solid electrolyte-based sensors. Solid electrolytes exhibit dominant ionic conductivity resulting from the migration of ions through point defect sites in the lattice. In these sensors electronic conduction (electrons or holes) only has a small contribution (typically less than 1%) to the total conductivity. The ionic transport number of solid electrolytes, which is defined as the ionic conductivity divided by the total conductivity, is typically greater than 0.99. [7]

2.1.1 Equilibrium potentiometric gas sensors.

A potentiometric sensor operates under open-circuit conditions where no electrical current flows through the external electrical circuit, thus preventing ionic current from flowing through the electrolyte. Potentiometric sensors have been classified by Weppner [8] into three types: (1) direct measurement of the mobile species (Type I); (2) indirect measurement of immobile components (Type II); and (3) analysis of other species by employing auxiliary solid phases (Type III). Type I sensor is the conventional potentiometric gas sensor which is made of two electrodes (reference and sensing) on each side of the electrolyte and directly measure the chemical potential difference of neutral components corresponding to the mobile species in the electrolyte. [9] An example of such sensors is an oxygen sensor with an oxygen-ion conductor, such as YSZ. Due to the lack of solid electrolytes with mobile ions originating from such gases as NO_x, SO_x, or CO_2, these types of sensors are typically used to detect oxygen. In Type II potentiometric gas sensors, gaseous analyte equilibrates with the component that differs from the predominantly mobile species. Consequently, the chemical potential of the conjugate (immobile) component in the electrolyte can be measured. For example, K_2CO_3 and Ag_2SO_4 solid electrolyte can be used to detect CO_2 and SO_3, respectively. [10, 11]. However, Type II sensors are still restricted by the limited number of suitable solid ionic conductors containing an immobile species with a known equilibrium reaction for the species to be detected. In addition, this type of sensor cannot be applied in a high temperature environment due to the lack of thermally stable solid electrolytes. To overcome the limitations of suitable electrolytes, Type III sensors were developed. In this type of sensor an auxiliary phase, which contains the same ionic species as those from the gas, is attached to the surface of the solid electrolyte. The auxiliary phase can be used to provide an equilibrium reaction between the target species and the ion that is mobile in the solid electrolyte, so that the voltage generated by the electrochemical cell is related to the concentration of

the target species. This allows solid cell gas sensors to detect a larger array of gases at high temperature, such as CO_2,[12] NO_x [13, 14] and SO_x.[15] The more detailed working principles of each type of potentiometric sensors were reviewed by Pasierb and Rekas [16].

2.1.2 Non-equilibrium potentiometric (mixed potential) gas sensors

Since suitable electrolyte or auxiliary electrode materials are not readily available, equilibrium potentiometric gas sensors are seldom reported to detect reducing gases (CO and HCs), especially at temperatures above 600 ^oC. In these cases, non-equilibrium approach may be employed as an alternative, in which gases are not in thermodynamic equilibrium at the interface between the electrode and the solid electrolyte. Usually more than one electrochemical reaction occurs at an electrode, so the resulting electrode potential becomes a mixed potential which is generated from a competition of the various reactions occurring at the electrode. [7] The configuration of mixed potential gas sensor is similar to equilibrium potentiometric gas sensor with two different electrodes. As previously mentioned, the potentiometric gas sensing mechanism is based on the establishment of a steady state in which all the electrons produced by an oxidation reaction are consumed by a reduction reaction. For equilibrium potentiometric sensors, oxidation and reduction reactions are the same reaction but in opposite directions, while for a mixed potential sensors the oxidation and reduction reactions are for different species. [17] Mixed potential type gas sensors can detect various target gases if the sensing electrode material is used properly. This type of gas sensor is particularly well-suited for detecting redox gases in combustion exhausts including CO,[18, 19] NO_x [20, 21] and HCs.[22]

2.1.3 Amperometric gas sensors

In contrast to potentiometric sensors, amperometric sensors are operated under an externally applied voltage which drives certain electrode reactions electrochemically. Usually the sensor signal is a diffusion limited current involving diffusion barriers. Each analyte molecule passing the diffusion barrier reacts immediately at the electrode while the reaction rate, reflected by the current at the sensing electrode, occurs at a thermodynamically determined potential for any given reaction. When operated under appropriate diffusion-limited conditions, the sensor current is simply proportional to the concentration of the analyte. The linear relationship between current and concentration typically

spans over 3 orders of magnitude. Measurements with high sensitivity (ppm to ppb) are achievable with excellent measurement accuracy under constant potential conditions. Compared to a potentiometric sensor which shows a logarithmic behavior to the concentration of gas and low sensitivity at high concentration, amperometric sensors is more suitable for the detection of high gas concentrations. With unique combined materials and appropriate designed geometries, amperometric gas sensors are capable of detecting a wide range of analytes, including O_2, H_2, CO, NO_x, SO_2, H_2S and organic vapors with electroactive functional groups likes alcohols or aldehydes. [23]

2.2 Resistive gas sensors

The resistor-type sensor based on semiconducting metal oxides is another commonly used gas sensor which possess advantages such as simple configuration, easy fabrication, cost effectiveness and also offers advances in miniaturization and MEMS (micro electronic mechanical system).[24] A semiconducting metal oxide serving as the sensing element is supported by an inert substrate and connected to two metallic electrodes or interdigitated electrodes. The resistor-type sensor measures the electrical resistance change of the semiconducting oxides due to the interaction between the sensing material and analyte gas, which typically involves an electron transfer. Based on the interactions between the sensing element and analyte gas, the semiconducting metal oxide-based sensors can be divided into three groups: (1) bulk conduction-based sensors, which are used to detect oxygen at high temperature (>500 ^oC); (2) surface conduction-based sensors, which are reported to show good sensitivity to reducing gases such as CO, H_2, and hydrocarbons (HCs) at low and medium temperature (200-500 ^oC); (3) metal/oxide junction based sensors, which are based on relative work function change, including metal-(insulator)-semiconductor (MS/MIS), Schottky diodes, metal-oxide-semiconductor capacitors and metal-oxide-semiconductor field effect transistors (MOSFET) at low and medium temperature (200-500 ^oC).[25] At high temperature (> 500 ^oC), most resistor-type sensors are reported to detect O_2 based on the bulk-conduction based mechanism. For other exhaust gas sensors (CO, NO_x, SO_x, HCs), they are mostly reported to follow the surface conduction mechanism in low and mild temperature (< 500 ^oC). However, a few metal oxides with lower conductivity and carrier mobility at high temperature, such as Ga_2O_3 and CeO_2, can be used to detect reducing gases (CO and HCs) at high temperature (>500 ^oC), which will be discussed in detail in the 'Resistive CO & HCs sensors' section.

2.3 Impedancemetric gas sensors

Another detection approach named "impedancemetric" employing AC measurements at a specified frequency has recently drawn increased attention. This approach is related to solid-state impedance spectroscopy - an electrochemical characterization technique that measures the cell response over a range of frequencies (typically from subhertz to megahertz).[26] The impedancemetric technique can be applied on either solid electrolyte-based sensors or semiconductor-based sensors. Solid electrolyte-based impedancemetric sensors have a similar design as mixed potential type sensors where instead of measuring voltage, a sinusoidal voltage is applied and the resulting current is measured. Impedance is then calculated as the ratio of voltage to current in the frequency domain. Impedance spectroscopy is a useful technique to investigate individual electrochemical components based on the frequency-dependent behavior by equivalent circuit analysis. In the case where electrochemical components (e.g., electrolyte, interface and bulk material) have significantly different time constant, these components can then be separated for individual analysis, which can be used to investigate the sensing mechanisms.[27, 28] Impedancemetric sensors based on YSZ have been reported for sensing gases such as water vapor,[29, 30] hydrocarbons,[31, 32] NO_x [27, 28, 33, 34] and CO [35]. Impedancemetric sensors can also operate in a resistor-type configuration for the detection of hydrocarbons without using solid electrolyte YSZ.[36, 37] Although impedancemetric sensor is the least developed sensor type, it exhibits several promising advantages, such as capability to measure total NO_x concentration, improved gas selectivity and accurate detection on single ppm level.

3. Recent progress in high temperature gas sensors

3.1 Oxygen sensors

Oxygen sensors used in automotive exhaust emission control systems are a major contributor for the applications of solid-state gas sensors.[5] The oxygen sensor is used to control the air/fuel (A/F) ratio that is fed to the engine, and in conjunction with a three-way catalyst, has led to a significant reduction in pollution emissions from automobiles. In addition, on-board diagnosis (OBD) requires a second oxygen sensor downstream to monitor the O_2 storage capacity of the catalyst which indicates the working efficiency. When the catalyst works efficiently, it stores oxygen while it reduces NO_x

during the lean cycle and releases oxygen while it oxidizes HCs during the rich cycle.[2] Therefore, O_2 sensors play an important role in combustion optimization, catalytic efficiency monitoring and emission reduction.

3.1.1 *Equilibrium potentiometric (Type I) oxygen sensors*

Potentiometric oxygen sensor, which is employed in the exhaust emission control system for the automobile engine, is one of the most successful applications of a solid-state sensor. The most abundantly used potentiometric oxygen sensor uses air as the reference gas electrode. According to the Nernst equation, the oxygen concentration can be determined by the open circuit potential (E), which is generated by the difference between the oxygen partial pressure at the reference electrode ($P_{O_2}^{\text{reference}}$) and that at the sensing electrode ($P_{O_2}^{\text{sensing}}$):

$$E = (t_{O^{2-}}) \cdot \left(\frac{RT}{4F}\right) \cdot \ln\left(\frac{P_{O_2}^{\text{sensing}}}{P_{O_2}^{\text{reference}}}\right)$$

where R is the gas constant, T is absolute temperature, F is Faraday's constant, and $t_{O^{2-}}$ is the transport number for oxide ions which is equal to one for a solid electrolyte. In high temperature applications, yttrium partly stabilized zirconia (YSZ) or its derivative is normally used as the solid electrolyte which is structurally and chemically stable up to 1600 °C. The conventional thimble-type YSZ-based oxygen sensor and planar type multilayer zirconia oxygen sensors have been systematically reviewed by Riegel.[5]

One major disadvantage of conventional YSZ-based oxygen sensors is the use of external Pt/air as the reference gas electrode, which impedes the miniaturization of those sensors. The bulky sensor configuration with external air reference electrode limits the location of measurement, which can only measure the oxygen concentration in the area near the wall of combustion chamber. If the external air reference electrode can be successfully removed, the potentiometric oxygen sensors, with smaller size and simpler configuration, can be positioned in the locations inside the combustion environment for more precise control. An alternative is to use metal/metal oxide as internal reference electrode, which can provide constant equilibrium oxygen partial pressure of the binary mixture at a fixed temperature. Several metal/metal oxide system have been investigated, including In/In_2O_3, Sn/SnO_2, Pd/PdO, Ru/RuO_2 and Ni/NiO [38-44]. Many of them can only work below or at 500 ^oC.

Among these studied metal/metal oxide system, the Ni/NiO reference electrode is the most promising internal reference system for high temperature applications. Chowdhury et al. have reported a Ni/NiO-based oxygen sensor which shows accurate and fast response with good recovery characteristics in the temperature range of 600-1400°C.[43] An Al_2O_3 isolation layer has been first employed in the design of an oxygen sensor to prevent high temperature alloy formation between Ni and Pt, leading to a significant enhancement in the performance and the stability of the sensor. However, after repeated tests over a longer period, the sensor performance degrades possibly due to grain growth and sintering of the inner electrode at high temperature. More recently, a durable Ni/NiO-based oxygen sensor were fabricated by a flexible and potentially low-cost method, which showed improved accuracy, as shown in Figure 1. The sensor exhibits good stability (> 5100 hrs), extended working temperature range (up to 663 ^oC), good tolerance to thermal and P_{O_2} cycling, fast response, high reproducibility and easy recoverability when Ni is depleted.[44] For metal/metal oxide-based oxygen sensor, tight sealing against oxygen penetration to solid reference electrode is highly challenging, which strongly affect the long-term stability of sensors at high temperature.

[Figure 1]

In order to avoid sealing issues, all-solid-state (only oxides) reference electrodes have been developed. Rajabbeigi et al. used solid CeO_2 (with 25 mol% ZrO_2) and CeO_2-ZrO_2-TiO_2 as reference electrode which stores oxygen at high temperatures acting as the reference O_2 source.[45-47] Though those sensors successfully responded to oxygen concentration change, they exhibited a narrower voltage (emf) at around the stoichiometric A/F ratio, compared to that using the conventional Pt/air reference electrode. Miura et al. have proposed a novel Mn_2O_3 reference electrode, which is completely insensitive to various exhaust gases, absolutely inert to change in oxygen concentration over a wide range and highly stable at elevated temperatures and in a harsh environment. [48] The planar sensor using Mn_2O_3 as reference electrode exhibited excellent responses to oxygen in the concentration range of 0.05–21 vol.% and gave negligible responses to other co-existing gases at 550 ^oC. The good performance of Mn_2O_3-RE-based oxygen sensors was similar to the result for tubular YSZ-based sensors using inner Pt as reference electrode, as compared in Figure 2, indicating that the using Mn_2O_3 as reference electrode can successfully achieve sensor miniaturization without sacrificing its performance. Thanks to elimination of air reference, this type of oxygen sensor is

low-cost and suitable for the mass production. However, the operating temperature of around 400-600 ^{o}C is relatively low. Therefore, more investigations and efforts are demanded to develop air reference free oxygen sensors at high temperature up to 1000 ^{o}C.

[Figure 2]

3.1.2 Amperometric (limiting current) oxygen sensors

For potentiometric oxygen sensors, the cell voltage depends logarithmically on the oxygen pressure. The stoichiometric point in the combustion process can be successfully measured with a potentiometric type oxygen sensor. However, potentiometric measurements are difficult in the lean combustion gas with a high concentration of oxygen. Therefore, a limiting-current measurement that gives a linear dependence on oxygen concentration is preferable for the detection of a wide range of oxygen concentrations. The basic working principle of amperometric oxygen sensors was discussed in a previous section. For a diffusion channel with length L and cross section A, the limiting current I_{lim} is given by: [49]

$$I_{\lim} = \frac{4FD_{O_2}P_{tot}A}{RTL} \cdot \ln(1 - x_{O_2})$$

Where D_{O_2} is oxygen diffusion coefficient, P_{tot} is total gas pressure, A is cross section of the diffusion channel, L is the length of the diffusion channel, and x_{O_2} is the molar fraction of oxygen in the gas. At oxygen concentrations below 10%, a linear relationship between oxygen partial pressure and limiting current holds to a good approximation with

$$I_{\lim} = -\frac{4FA}{RTL} \cdot D_{O_2} \cdot P_{O_2}$$

The current output of these devices increases linearly with increasing oxygen concentration under suitable temperature and applied polarization voltages. Measurements with high sensitivity (ppm to ppb) can be achievable with excellent measurement accuracy. [23] However, the major disadvantage of amperometric sensors is their poor thermal and long-term stability as well as the difficulty in designing a suitable diffusion barrier, which determines the behavior of the sensor.[50]

At high operating temperature, besides YSZ which is one of the major solid electrolytes, Gd or Sm

doped CeO_2 have been considered to be promising alternative solid electrolytes. $Ce_{0.8}Sm_{0.2}O_{1.9}$ (CSO) has been reported to be employed as solid electrolyte in amperometric oxygen sensor at 500-700 ^oC, due to its higher ionic conductivity than YSZ. [51, 52] In terms of diffusion barrier material, which is required to have high electronic conductivity and good thermal stability, lanthanum strontium manganate (LSM) is found to exhibit good diffusion control for the amperometric sensors. LSM is a mixed ionic-electronic conductor for oxygen membranes, and cobalt containing perovskites (LCO) shows even better properties, such as high electronic conductivity, high oxygen ion conductivity and high electrochemical catalytic activity. A dense diffusion barrier amperometric oxygen sensor with CSO solid electrolyte and $La_{0.8}Sr_{0.2}Co_{0.8}Fe_{0.2}O_3$ (LSCF) dense diffusion barrier has been reported, as shown in Figure 3, which shows a good limiting current platform and linear response when the oxygen volume fraction is from 0 to 0.21 at 700 ^oC.[52] The limiting current remains constant after the sensor is continuously tested for 60 h, which indicates relatively good long-term stability.

[Figure 3]

In addition to devices based on a single amperometric cell, more sophisticated devices combining several cells may increase the accuracy of measurements or perform several functions.[53] For example, one cell is operated in the amperometric mode and works as oxygen pump, while the other is operated in the potentiometric mode and works as oxygen gauge. [54] There are limited literatures reporting high temperature amperometric oxygen sensors, probably due to their disadvantages such as a more complicated packaging and design, greater difficulty in controlling the diffusion barrier and lack of long term durability.

3.1.3 Resistor-type oxygen sensors

Another type of oxygen sensor that has been developed for harsh environment applications is the resistor-type oxygen sensor. Compared to solid electrolyte-based oxygen sensors, the advantages of resistor-type oxygen sensors are their simple configuration, easy fabrication, cost effectiveness and miniaturization capability. Resistive oxygen sensors are generally based on the bulk conduction mechanism at high temperature above 800 ^oC. The bulk defects of metal oxides are usually associated with oxygen ion vacancies, metal ion interstitials and vacancies, electrons and holes. Semiconducting metal oxides usually exhibit conductivity which changes with the varied concentration of the charge carriers – electrons (n-type) or holes (p-type). At high temperatures of

700-1100 ^{o}C, the bulk defect species have high mobility, allowing the non-stoichiometric oxide to reach equilibrium by reacting with the gas species in the surrounding atmosphere, leading to a change in the charge carriers' concentration.[25] Hence, the bulk conductivity of the metal oxide depends on the composition of the ambient gas species, which can be used to determine the concentration of the analyte gas. For the oxygen sensing mechanism of n-type semiconductors, the oxygen vacancies ($V_O^{\bullet\bullet}$) in the bulk oxide can react with the oxygen molecules in the gas phase (O_2) and incorporate two electrons to produce a lattice oxygen (O_O^x). A reverse process can also occur depending on the oxygen partial pressure, which can be expressed as:

$$O_O^x \leftrightarrow V_O^{\bullet\bullet} + 2\,e^{'} + 1/2\,O_2$$

Based on the above reaction increasing oxygen partial pressure can reduce the concentration of electrons in n-type metal oxides, resulting in the decrease of bulk conductivity. The well-established relation between the electrical conductivity (σ) and the oxygen partial pressure (P_{O_2}) can be expressed by:

$$\sigma = A\exp\left(-\frac{E_A}{KT}\right)P_{O_2}^{1/m}$$

where E_A is the activation energy which represents the sensitivity of the electrical conductivity to changes in temperature.[55] This equation is valid for both p-type and n-type semiconductors which can be indicated by the sign of 1/m, which is positive for p-type (hole) and negative for n-type (electron) semiconductors. The absolute values of 1/m depend on the dominating defects involved in the reaction between oxygen gas and the sensing material, typically varying between 4 and 6. With lower absolute values of m, the sensor exhibits greater sensitivity to the change of oxygen partial pressure. Therefore, it is very important to select semiconducting metal oxides with small m and E_A to obtain high oxygen sensitivity and low interference to temperature fluctuation.

Over last several decades, titanium dioxide (TiO_2), niobium pentoxide (Nb_2O_5), gallium oxide (Ga_2O_3), cerium oxide (CeO_2) and perovskite strontium titanate ($SrTiO_3$) have been extensively studied as resistive oxygen sensing materials. Among them, TiO_2 is one of the most widely studied semiconductors which has high sensitivity to oxygen within a wide range of oxygen partial pressure

(P_{O_2}: 1-10^{-30} atm). [56] Nb_2O_5 is reported to be able to detect oxygen up to 800 ^oC with minimal interference from CO, CH_4 and humidity. However, the response time is long (5 min).[55] Ga_2O_3 is another promising material for oxygen sensing with higher thermal stability which can be operated in temperature ranges from 850-1000 ^oC.[57] CeO_2 also has good stability up to 1000 ^oC and exhibits a large diffusion coefficient for oxygen vacancy compared with TiO_2, resulting in quick changes of oxygen vacancy concentration in equilibrium state and thus fast response.[58-60] In addition, CeO_2 possesses higher resistance to corrosive gases (Cl_2, SO_2 and NO) compared with $SrTiO_3$ and Ga_2O_3.[59, 61] $SrTiO_3$, belonging to perovskites, which have high melting and decomposition temperature, is stable up to a temperature of 1400 ^oC. [62] $SrTiO_3$ shows an n-type behavior in the oxygen partial pressure below 10^{-5} atm (1 Pa) and transforms to a p-type semiconductor at higher oxygen partial pressure with the oxygen sensitivity factor m = ± 1/4 at 800 ^oC. The sensing performance of some high temperature resistive oxygen sensors are summarized in Table 2.

[Table 2]

Although all of these materials exhibit promising potential as sensitive resistor-type oxygen sensor at high temperature, one disadvantage that obstacles their real application is the high temperature dependency of the conductivity. In order to decrease the temperature dependence of the sensor output, two approaches have been proposed to develop temperature independent resistive oxygen sensor. One is the use of an additional temperature compensating material and another is the use of a sensitive material which has an intrinsic temperature independent conductivity. Temperature compensating materials (TCMs) should be insensitive to the oxygen partial pressure, but should have similar temperature dependence to the oxygen partial pressure measurement materials (OMM). Izu et al. have reported a series of OMM and TCM combinations, including non-doped CeO_2 and $Ce_{0.9}Y_{0.1}O_{2-\delta}$ [63], $Ce_{0.95}Zr_{0.05}O_2$ and $Zr_{0.7}$ $Y_{0\cdot3}O_{2-\delta}$ [64], $Ce_{0\cdot9}Zr_{0.1}O_2$ and $Ce_{0.5}Y_{0.5}O_{2-\delta}$ [65]. For each OMM they investigated, different compositions of TCM have been systematically studied to achieve the best compensation, which should have the same activation energy of resistance with OMM but independent sensitivity to oxygen partial pressure. Those sensors exhibited approximately independence of the temperature in their investigated temperature range, typically from 500 to 800 ^oC. In a recent report, temperature independent ZrO_2-doped CeO_2-based (ZDC) resistive oxygen sensor within a temperature range of 650–950 ^oC was fabricated from precipitated ceria–zirconia

solid solution powders. [66] Two ZDC films containing 10 at% and 5 at% ZrO_2, whose activation energies were approximately equal, were used as OMM and TCM, respectively. This sensor shows extremely good temperature-independence with a relatively good sensitivity and stability, as presented in Figure 4.

[Figure 4]

Besides the temperature compensation materials discussed above, another group of perovskite material is found to have good sensitivity to oxygen partial pressure and intrinsic temperature independent conductivity, which can be employed to fabricate temperature dependent resistive oxygen sensor. Up to date, only a few perovskite have been found that show a low or even negligible temperature dependency of conductivity. $SrTi_{1-x}Fe_xO_{3-\delta}$ (STF) and doped STF are the most widely studied systems. One of the most promising materials is $SrTi_{0.65}Fe_{0.35}O_{3-\delta}$ (STF35), which is sensitive to the oxygen partial pressure but shows no cross-sensitivity to temperature fluctuations. [67] The study of temperature coefficient of resistance (TCR) behavior of $SrTi_{1-x}Fe_xO_{3-\delta}$ with varied Fe concentration was carried out by Rothschild et al. [68] The results reveals that for STF35 the bandgap energy is such that the Fermi energy lies just at the right distance from the valence band in order to compensate for the temperature-dependence of the mobility, yielding a zero TCR from the product of the free carrier (holes) concentration and mobility terms. Conductivity of STF as a function of oxygen pressure at different temperatures and STF compositions are presented in Figure 5. In addition, STF60 [69, 70] and doped STF like $La_{0.05}Sr_{0.95}Ti_{0.65}Fe_{0.35}O_{3-\delta}$ [71, 72] and $(Sr_{0.95}La_{0.05})[(Ti_{0.7}Fe_{0.3})_{0.95}Ga_{0.05}]O_{3-\delta}$ [73] were also investigated as temperature independent resistive oxygen sensor. Although those sensors show good oxygen sensing performance, STF-based materials are prone for sulfur oxide poisoning. [74] Besides STF-based perovskite, there are also other sensing materials that have been investigated, such as $BaFe_{1-x}Ta_xO_{3-\delta}$ [75] and $LaCu_{1-x}Fe_xO_{3-\delta}$ [72, 76]. $LaCuO_{3-\delta}$ is known for its excellent temperature-independent properties, but the material is not stable at high temperatures and under reducing conditions. By partially substituting Cu with Fe, thermal and chemical stability can be improved without deteriorating temperature independency.

[Figure 5]

The research on resistive oxygen sensors has been conducted for several decades, from largely materials screening to addressing the issue of temperature dependence, sulfur resistance and reducing

atmospheres resistance. More efforts are needed to further improve the reliability and long-term stability of resistive oxygen sensors for practical high temperature application.

3.2 Combustibles (CO and HCs) sensors

Solid-state oxygen sensors are widely used in applications of combustion process control. To cope with more stringent pollutant emission regulations, other gas sensors are also devised to measure regulated species such as CO and unburned hydrocarbons (HCs). This is a difficult task since detection concentration as low as a few ppm and operation temperatures as high as 800-1000 ^{o}C are needed for future combustion control strategies and on-board diagnosis. CO is formed when carbon in fuels is not fully burned. *In-situ* monitoring of CO can determine the fuel combustion efficiency directly and provide the feedback to control systems. Unburned hydrocarbons are another important gas targeted in rich combustion conditions. For direct OBD purposes, high temperature hydrocarbon sensors employed downstream of a three-way catalytic converter (TWC) can measure the limited components directly, which can provide more precise measurements than dual oxygen sensors (indirectly determining oxygen storage capacity). [77] In gasoline direct injection engines hydrocarbon sensors can detect the end of the regeneration phase more precisely than a λ sensor and they can also be used for OBD of close-coupled oxidation catalysts.

3.2.1 Resistor-type CO& HCs sensors

The most common sensor for CO and hydrocarbon detection is a resistor-type sensor at low or mild temperature (300-500 ^{o}C), which detect analytes in an atmosphere of fixed oxygen partial pressure (air) based on the adsorption and desorption of gas species on the metal oxide surface. At high temperature (>500 ^{o}C), strong reducing gases (CO and HCs) can react with the lattice oxygen to form oxygen vacancies in the oxides, which makes it extremely challenging for resistor-type sensors to detect CO and HCs with good recoverability, reproducibility and stability. Therefore, only a few reported metal oxides with lower conductivity and carrier mobility at high temperature can be used to detect reducing gases (CO and HCs) in high temperature environment.

As illustrated in Figure 6, depending on temperature and carrier mobility of oxides, the interaction between gas phase and oxides can be described as follows: I) direct chemisorptions of reducing gas on the surface resulting in injection of electrons into the solid (Figure 6: Top); II) surface reactions

which lead to the formation of oxygen defects located at the surface of metal oxides (Figure 6: Center); III) crystal defect equilibrium changes due to inner lattice oxygen atom transferring to the surface (Figure 6: Bottom). Defect equilibrium (mechanism III) can only occur if the operating temperature is high enough to gain high defect mobility. Sensor response arises due to gas-induced changes of the carrier density by surface effects involving charged chemisorption or surface reactions. [78] For such high temperature resistive CO and HCs sensor, the carrier mobility is not influenced by the grain boundaries, instead it is directly determined by the crystal lattice which greatly improved the reproducibility of the sensor.[79]

[Figure 6]

To the best of our knowledge, CO and HCs detection based on resistor-type sensor at high temperature above 600 ^{o}C have been seldom reported in the literature. The studies at operating temperature higher than 800 ^{o}C are even fewer. Ga_2O_3 is one of reported material can be used to detect CO and HCs at high temperature. Ga_2O_3 is widely used for the detection of O_2, which is generally operated with the bulk-volume-defect in equilibrium at temperatures between 900 and 1000 ^{o}C. At lower temperatures, the volume-defect-equilibrium is not attainable and surface effects dominate the sensor's response.[80] Fleischer et al. investigated the CO and HCs sensing properties of pure Ga_2O_3 and doped Ga_2O_3 in the temperature range of 600-1000 ^{o}C [81-84] The sensors based on Ga_2O_3 and SnO_2 doped Ga_2O_3 show stable, sensitive and recoverable response towards both CO and HCs, however it suffers from high cross sensitivity. [82] With the gold dispersion, Ga_2O_3 exhibits enhanced sensitivity to CO. [83] They also reported that with increasing operating temperature the sensitivity of the resistor-type sensor decreases. Therefore, sensitivity of the sensor at high temperature is an important factor to evaluate the sensing performance. More recently, electrospun CeO_2 nanofibers (d~ 376 nm) was reported to be able to detect CO in N_2 at 800 ^{o}C and 1000 ^{o}C with excellent sensitivity, as well as good stability, recoverability and reproducibility, as shown in Figure 7. [85] This is one of few reported high temperature sensors utilizing nanostructured material. The developed sensor also possesses the highest sensitivity among resistor-type CO sensors operated at such high temperature.

[Figure 7]

Besides the sensitivity of the sensor at high temperature, selectivity is the most challenging issue due

to the intrinsic sensing mechanism. Dutta et al. have been investigated TiO_2 (in both anatase and rutile form) based resistive CO sensors above 600 ^oC.[86-89] Anatase behaved as an n-type semiconductor, showing considerable sensitivity towards both CO and CH_4. CuO was added to increase the sensitivity toward CO and La_2O_3 was used to inhibit the anatase to rutile transformation. This anatase/ La_2O_3/ CuO-based sensor shows good selectivity to CO and negligible response to CH_4, which can be ascribed to the efficient catalyzed CH_4 oxidation on CuO surface leading to lack of CH_4 reaction on the anatase surface.[87] Contrary to anatase, rutile exhibited p-type conductivity. Anatase-rutile (n-p) composites with varied compositions were investigated to achieve good selectivity to CO over CH_4 at the temperature of 600 ^oC. In the sample with 75% rutile, both n- and p-pathways would percolate, resulting in diminished changes in resistance. Since the overall response of CH_4 was smaller than that of CO, after the responses from anatase and rutile were cancelled out, the sample with 75% rutile showed n-type response to CO while no change upon exposure to CH_4, indicative of a selective CO sensor. [88] Furthermore, to fabricate a selective hydrocarbon sensor, Dutta et al. have employed Pt-zeolite as a catalytic filter layer, which converts CO into CO_2 and HCs into CO_2 and water. [90] Anatase, serving as sensing material, is not sensitive to CO_2 but only shows the response to water from hydrocarbon oxidation at 600 ^oC. Thus, the Pt-zeolite filter-TiO_2 sensor can respond selectively to HCs in the presence of CO. The limited reports on various resistor-type high temperature combustible sensors are summarized in Table 3.

3.2.2 Mixed potential CO & HCs sensors

Most solid electrolyte-based CO or hydrocarbon sensors under development use the mixed potential principle. The electromotive force (emf) between two different electrodes located on a solid electrolyte is the sensor signal. Usually, one electrode is made of a catalytically active conductor such as platinum while a catalytically inactive material such as gold serves as a counter electrode. YSZ is the most widely used solid electrolyte and there are also a few reports based on β-alumina [91] or $Ce_{0.8}Ga_{0.2}O_{1.9}$ (CGO) [18, 92, 93]. For a mixed potential sensor, differences among electrolytes depend primarily on the reaction kinetics at the three-phase boundary rather than on the conduction properties of the electrolyte. Since these sensors are operated in non-equilibrium, with increasing temperature the system will approach equilibrium leading to an output decrease. Therefore, most of mixed potential sensors operate in the range of 500-600 ^oC. Solid-electrolyte based CO and HCs

sensors were the subject of the review paper authored by Fergus. [94] Again, the focus of our review article is on the solid-state gas sensors which can be operated at high temperature above 600 ^{o}C represented by papers collected in Table 3.

Most investigations of mixed potential CO and HCs sensors focused mainly on screening electrode materials. Some simple oxides, such as WO_3 [95, 96], Nb_2O_5 [19, 97, 98] and Nb_2O_5-Ta_2O_5 [99] were investigated as sensing electrode for CO/HCs detection at 500-700 ^{o}C by Di Bartolomeo's research group. For CO detection, WO_3-based sensor [(Au)Pt/YSZ/Pt(Au)/WO_3] shows considerable response towards NO_2 in opposite direction, while Nb_2O_5-based sensor [Pt/YSZ/Nb_2O_5] exhibits higher sensitivity towards hydrocarbons than CO, especially sensitive to propylene at 700 ^{o}C. Zosel et al. have been studied sensing performance of a series of YSZ-based HCs sensors using Au-oxides composite as sensing electrode at 700 ^{o}C with Ga_2O_3, Y_2O_3, Al_2O_3, ZrO_2, In_2O_3 and Nb_2O_5 as oxides.[100-102] Au-oxide composite electrodes using Nb_2O_5, Ga_2O_3, In_2O_3 as oxides showed, as compared with pure gold, an enhanced propylene sensitivity, while those with Y_2O_3, Al_2O_3, ZrO_2 tended to the equilibrium behavior. The HCs sensitivity of Au-oxide composite electrode increases in the direction: Y_2O_3, ZrO_2, In_2O_3, Ga_2O_3, and Nb_2O_5, which correlates very well with the catalytic activity of these materials for the hydrocarbon combustion. The more inactive the material the better is the HC sensitivity of the electrode prepared with that material.

Besides simple oxides, doped-oxides and perovskites have also been explored. Mixed potential CO sensor, coupling scandia-stabilized zirconia (ScsZ) as electrolyte and tin-doped indium oxide (ITO) as sensing electrode [ITO/ScSZ/Pt], has been fabricated by Kale et al. for CO detection. [103-105] This sensor shows excellent sensitivity to CO at low concentration; however it still suffers from interfering gases like NO_2, CH_4 and O_2. Brosha et al. have been investigated different perovskites as electrode material for CO/HCs sensor.[106-108] $LaCoO_3$ and $La_{0.8}Sr_{0.2}CoO_{3-\delta}$ thin films have been employed as sensing electrode with YSZ electrolyte and Au counter electrode for CO and HCs detection at 700 ^{o}C. [106] Due to the instability of Au morphology which jeopardizes device-to-device reproducibility, a second metal oxide thin film, doped $LaMnO_3$, was used to replace Au electrode, resulting in better stability. Another mixed potential device using $Y_{0.16}Tb_{0.30}Zr_{0.54}O_2$ (TbYSZ) and $LaMnO_3$ as two electrodes [Au/$LaMnO_3$/YSZ/TbYSZ/Au] showed a high mixed potential response to CO and HCs at 600 ^{o}C, however, lifetime testing over a 3000 h time period indicated that aging

took place.[107] In addition, spinel $NiCr_2O_4$ and $ZnFe_2O_4$ were also explored as sensing electrodes of YSZ-based HCs sensor with Pt as counter electrode, which showed preferential sensitivity to HCs and small sensitivity to NO_2 at 600 ^oC.[108]

Due to the mechanism of mixed potential sensors, most of them suffer from poor selectivity. Both CO and hydrocarbons can be oxidized to produce electrons for the reduction of oxygen, mixed potential CO/HCs sensors usually have high cross sensitivity. Besides, the interference also comes from the change of NO_2 and O_2 concentration. As the magnitudes of the responses to different gases are different for different electrodes, CdO [109] and NiO-Au [110] composite have also been employed by Miura et al. as sensing electrode for selective C_3H_6 detection at 600 ^oC. The sensors showed good selectivity to C_3H_6 over CO, CH_4, C_3H_8, NO and NO_2, as show in Figure 8A. The sensitivity (Δemf) of NiO-Au composite-based sensor was also found to be independent of water vapor concentration in the range of 2–11 vol% in the sample gas. More recently, YSZ-based sensor utilizing Zn–Sn–O composite as sensing electrode exhibited a preference to CO than C_3H_8 and NO_2, while the one using $ZnCo_2O_4$ as sensing electrode indicated excellent selectivity to C_3H_8 over CO and NO_2 at 600 ^oC, showing in Figure 8B and 8C.[111] In addition to developing new materials with good selectivity, novel sensor design is also another approach to improve selectivity. A hydrocarbon sensor consisting of a gas-detection cell and an oxygen pump cell have been invented by Inaba et al. [112] They used Pt as active electrode and Pr_6O_{11} as inactive electrode which were formed on YSZ by sputtering. At 800 ^oC, the gas-detection cell showed high output sensitivity for hydrocarbon gases such as CH_4 and C_3H_8 and low sensitivity towards H_2 and CO, indicating its good selectivity. The results are exhibited in Figure 9. The electric potential generated on the Pr_6O_{11} electrode was almost the same as the potential at the Pt electrode in O_2–H_2 and O_2–CO atmospheres (Figure 9A), leading to reduced sensitivity to H_2 and CO. In addition, the output of the sensor is greatly enhanced by using a pump cell to decrease the oxygen concentration in the gas-detection space. Therefore, it was suggested that by controlling the oxygen concentration in the gas-detection space, it possible to detect trace amounts of hydrocarbon gases, even in a high oxygen concentration atmosphere.

[Figure 8] [Figure 9]

Although there are a number of novel materials and techniques for improving selectivity, each approach may not completely eliminate all interference. For most mixed potential sensors, selectivity

is still a major challenge. Therefore, sensor arrays, combined with technologies for pattern recognition and data analysis, will likely be required to identify individual species in complex unknown gas mixtures.

[**Table 3**]

3.3 Nitrogen oxides (NO_x) sensors

The development of high temperature NO_x sensors also plays a role in mitigation of environmental and health concerns and the optimization of combustion processes. NO_x is known to be one of the main causes of acid rain and NO_2 can cause damage to human nerve and respiratory systems. Combustion exhaust contains 7–80% NO in total NO_x content, corresponding to 60-3,000 ppm, due to its stability at high temperature (>500 °C) [1]. It is therefore important to detect NO as well as NO_2 in harsh exhaust conditions for emission control. NO_x storage catalysts (NSC) for novel gasoline direct injection engines and selective catalyst reduction (SCR) systems for NO_x mitigation in diesel engines also promote the desire of developing NO_x sensors for combustion processes. Gasoline direct injection (GDI) engines are designed to improve fuel efficiency and reduce NO_x and CO_2 emissions from engine during the lean phase, or reduce CO and HCs emissions during the rich phase by using NO_x stored from the lean phase to oxidize the reducing gases. GDI engines need NSC to store NO_x during the lean phase for 2 min and then release NO_x to react with reducing gas in rich phase (also called regeneration phase), usually in a few seconds. This complex process requires a reliable NO_x sensor that is mounted downstream of NSC to determine increasing NO_x emissions, indicating that NO_x-storage capacity is exhausted. Therefore, the requirements for NO_x sensors to be used in the commercial combustion application are summarized in literature [113] as follows: 1) the sensors must withstand high temperatures (600–900 ^oC) for a long duration of time, 2) the sensor should be insensitive to moisture content and be able to provide stable signals even in the absence of oxygen.

3.3.1 Amperometric NO_x sensors

The most successful NO_x sensor is the commercially available amperometric sensor. This sensor consists of two chambers with the functions of O_2 removal and NO detection. In the first chamber, the O_2 found in automobile exhausts are extracted by means of an oxygen pump. In the second chamber, NO is decomposed into N_2 and O_2 and the O_2 is detected by an amperometric

zirconia-based type sensor. Although these sensors measure NO_x concentration accurately and have been shown to operate for long periods of time with only moderate degradation in the signal, they have not been widely used due to their high cost and complex design.[114] Therefore, a number of investigations still focus on electrode and electrolyte materials for amperometric NO_x sensor. Miura et al. employed $CdCrO_4$ as sensing electrode in YSZ-based amperometric sensor for NO and NO_2 detection at 500-600 ^oC. [115, 116] Ishisara et al. used doped-$LaGaO_3$ as electrolyte and different compositions of Ni-doped $La_{1-x}Sr_xMnO_3$ (LSMO) as active and inactive electrodes to selectively detect NO at 500-700 ^oC. [117-119] Those sensors were found to possess good sensitivity and little cross-sensitivity to coexisting gases, e.g. CO, H_2, C_3H_6, CO_2, H_2O and NO_2. In order to minimize the interference from O_2 in background, La-Sr-based perovskite oxides were studied as sensing electrodes with YSZ as solid electrolyte by Takahashi et al., which preferentially reduce NO_x in the presence of excess O_2.[120, 121] It was reported that the sensor using $La_{0.6}Sr_{0.4}Co_{0.98}Mn_{0.02}O_3$ showed high response to NO_2 at 550 ^oC, however it still was slightly affected by the changes in O_2 concentrations. [120] In another report, multi-metallic electrodes were investigated for amperometric NO gas sensor.[122] The sensor (RhPtAu/YSZ/RhPtAu) showed a linear response to NO concentration with sensitivity of ~14 nA/ppm and was nearly independent to O_2 concentration with negligible sensitivity of 0.02 nA/ppm at a constant potential of −400 mV at 600 ^oC, implying the possibilities for the development of a highly sensitive amperometric NO gas sensor without oxygen pumping in the sensor design. For high temperature automotive application, the NO_x sensors should be capable of keeping good response and selectivity above 700 ^oC. However, only a few NO_x sensors that can be used at temperature above 700 ^oC have been reported, especially for amperometric sensors. A new-type amperometric sensor was recently fabricated by using YSZ as electrolyte and a nano-structured perovskite-type oxide $Gd_{0.2}Sr_{0.8}FeO_{3-\delta}$ (GSF) impregnated on porous YSZ as sensing-electrode (SE).[123] As shown in Figure 10, the fabricated sensor was found that the response current was almost linear to NO_2 concentration from 25 to 500 ppm with high sensitivity of 2.61 μA/ppm at 800 ^oC when SE was polarized at -400 mV. The sensor also showed good reproducibility, stability and good selectivity against O_2 and CO_2, which was only studied at 500 ^oC. Further studies are needed for the long term stability and selectivity in the presence of CO and hydrocarbons.

[**Figure 10**]

Besides amperometric NO_x sensors, resistor-type sensors based on WO_3 were also used for measuring NO_x at high temperatures;[124, 125] however, these sensors do not possess the necessary selectivity and stability. The fundamental problem with equilibrium potentiometric NO_x sensors is suitable materials are not readily available for high temperature operation, including electrolyte materials with the desired conduction properties and stable auxiliary electrodes. Therefore, mixed potential sensors are devised to overcome this issue by using galvanic cells consisting of electrode materials with different catalytic activities.

3.3.2 Mixed potential NO_x sensors

Mixed potential NO_x sensors have been intensively reviewed. [114, 126] In order to satisfy the requirements for high temperature sensing, it is vital for NO_x sensors to have a sensing material with excellent thermal stability. There have been many metal oxides which were explored as potential sensing electrodes. Most of the sensing materials for mixed potential NO_x detection operating above 600 ^oC are summarized in Table 4. Miura's research group has been extensively investigated mixed potential NO_x sensors for high temperature application for over 20 years. In earlier years, WO_3, [20, 95, 96, 127] $NiCr_2O_4$, [128] $ZnFe_2O_4$,[129] $ZnCr_2O_4$ [21, 130, 131] and ZnO [132] were studied for NO and NO_2 detection at 600-700 ^oC. Those sensors showed responses to NO and NO_2 in opposite direction with different sensitivity, which are shown in Table 4. Again, since the sensor relies on non-equilibrium conditions, a decrease in response with increasing temperature is expected. NiO and Ni-family oxides are found be to the most promising material for ultra-high temperature sensing electrodes above 800 ^oC. Mixed potential sensor based NO_x sensor attached with NiO sensing electrode was well characterized and employed for high temperature NO_2 detection in the operating temperature range of 800–900 ^oC. [133-136] The NiO electrodes showed good sensitivity in wet atmospheres, as well as in dry atmospheres. The sintering temperature and film thickness affects the sensing performance. [137, 138] It was reported that the sensor using the thin NiO-SE (120 nm) exhibited always higher NO_2 sensitivity than that attached with thick NiO-SE fabricated by screen-printing technique. Temperature dependence of NO_2 sensitivity of NiO-SE was also investigated lately.[139] Figure 11A presents the sensing response of various oxide sensing electrodes to 400 ppm NO_2 at 850 ^oC. [136] NiO gives the highest NO_2 sensitivity and also has the highest sensing temperature according to Table 4. The improvement in sensing characteristics of NiO based mixed potential NO_x sensors can be achieved by an addition of

a noble metal to NiO sensing electrode. Among the various noble metals (Pt, Rh, Ir, Pd and Ru) examined, Rh was found to give a significant enhancement in NO_2 sensitivity, as shown in Figure 11B. [140] In addition, other oxides, like CuO [141] and WO_3 [142], were also employed to modify the NiO-based sensing electrode. WO_3 was found to give a significant enhancement in NO_2 sensitivity at 800 ^oC. Figure 11C presented comparison of sensitivity for the sensors using NiO-SE doped with various metal-oxide additives at 800 ^oC. A follow-up research reports that a hetero-oxide sensing electrode (Cr_2O_3 on NiO(+WO_3)) was found to be able to detect NO_2 selectively at 895 ^oC.[143] It was speculated that the additional oxide layer (Cr_2O_3) placed on the NiO (+WO_3) layer acted as a catalyst for the oxidation of CO, hydrocarbons and NO and led to better NO_2 selectivity. Furthermore, chromium and cobalt were doped in nickel oxide in order to further improve the sensing performance. $Ni_{0.95}Cr_{0.03}O_{1-\delta}$ improves the recovery rate with a slightly reduced sensitivity. [144] The sensor attached with a $Ni_{0.9}Co_{0.1}O$-SE achieved the maximum improved sensitivity and $Ni_{0.8}Co_{0.2}O$ SE showed excellent selectivity to NO_2 with acceptable sensitivity. [145] As illustrated in Figure 11D, Co doping in NiO resulted in a large decrease in the rate of anodic reaction of O_2 which tended to increase sensitivity on one hand; on the other hand, it also led to a sensitivity decrease due to a higher degree for gas-phase decomposition of NO_2 to NO. Trading-off of these two effects, $Ni_{0.9}Co_{0.1}O$-SE showed highest sensitivity and $Ni_{0.8}Co_{0.2}O$-SE exhibited a moderate sensitivity to NO_2. In addition, the reducing gases (CO, NO, and hydrocarbons) are almost oxidized during the diffusion process through the $Ni_{0.8}Co_{0.2}O$-SE matrix before arriving at the SE/YSZ interface, resulting in an excellent selectivity to NO_2. The sensor attached with $Ni_{0.9}Co_{0.1}O$-SE also showed excellent long-term stability for about 6 months.

[**Figure 11**]

One can conclude from above, that most researches of mixed potential NO_x sensors have focused on electrode materials. However, besides the intrinsic chemical properties of SE material, the sensor configuration and fabrication method can largely affect the mixed potential sensing performance. For mixed potential sensor, the density of three-phase boundary (TPB) sites is a very important parameter which influences the behavior of the electrode and sensing performance. Electrodes with a high number of TPB sites are expected to provide faster sensing response and longer lifetimes.[146] As mentioned previously, most investigation of mixed potential sensors focused mainly on new

electrode materials, but the effect of the TPB microstructure on the sensing performance was generally ignored. In recent research, microstructures of sensing electrodes related to the effect of TPB sites have been attracting more attention. It was reported by Lu et al. that sensing performances of a mixed potential NO_2 sensor based on YSZ and NiO SE was improved by modifying the TPB.[147] Hydrofluoric acid with different concentrations (10%, 20% and 40%) was used to corrode YSZ substrate to obtain large superficial areas of TPB. As presented in Figure 12B and 12C, the YSZ plate corroded with 40% hydrofluoric acid has the largest superficial area, correlating to the largest number of TPB sites, which also gave the highest sensitivity towards NO_2 up to 76 mV/decade at 850 ^oC. In addition, the sensor also displayed high selectivity and speedy response kinetics to NO_2. Lately, another similar result can be found in a report of porous YSZ-based sensor attached with $MnCr_2O_4$ SE. [148] YSZ-substrate was modified by double-tape casting and pore-forming method. It was confirmed by SEM that the YSZ substrate prepared by using the slurry with 15 wt% starch (highest concentration) had the largest contact area of TPB. The mixed potential $MnCr_2O_4$ SE-based sensor using porous YSZ substrate with largest contact areas showed the largest response to NO_2 at 800 ^oC compared with other sensors.

[**Figure 12**]

Other than sensitivity and selectivity of mixed potential NO_x sensor, another challenge is the difficulty to measure the total amount of NO_x ($NO+NO_2$) required by automotive application. The opposite dependence on NO and NO_2 would result in response compensation in real exhausts emitted by vehicles. One way to solve this problem is to convert NO_x into NO_2 before the measurement takes place by using an oxidation catalyst electrode [126].

3.3.3 Impedancemetric NO_x sensors

Among all types of NO_x sensors, impedancemetric NO_x sensors are the least developed. These sensors have shown promise in detecting NO_x at lower ppm levels[114] and unlike mixed potential sensors, the response of impedancemetric sensor to NO and NO_2 are of the same sign and similar in magnitude, indicating that it can be used to measure the total amount of NO_x. The recent progress of impedancemetric NO_x sensors was reviewed by Rheaume.[149] Most research groups use the change in modulus at a specific frequency (typically $f \leq 10$ Hz) as the metric for sensitivity. Miura et al.

originally proposed an impedancemetric YSZ-based NO_x sensor with a $ZnCr_2O_4$ sensing electrode, which can detect the total concentration of NO_2 and NO.[28, 150] The sensor sensors show almost same sensitivity towards NO and NO_2 at 700 ^oC, as shown in Figure 13A. Equivalent circuit model (Figure 13B) was proposed for this senor to investigate the sensing mechanism. The impedance spectra in NO_x and air can be fitted by model simulation. Different elements in the model represent different parts of the sensor. In Figure 5B R_b represents the YSZ-bulk resistance, R_o and C_o are resistance and capacitance of oxide electrode respectively, while R_i and C_i represent resistance and capacitance of the interface between YSZ and the oxide electrode respectively. Based on the difference between the impedance spectra in NO_x and air, one can conclude that only the electrode-interface resistance (R_i) is affected by the interaction between the interface and NO_x gas, such as adsorption and reactions. In a follow-up report, the relation between the thickness of $ZnCr_2O_4$ films and the performance of impedancemetric NO_x sensor was investigated, showing that large thickness (39 μm) of sensing electode was beneficial for total NO_x detection at 700 ^oC, which is shown in Figure 14A and 15B. [131] Due to gas-phase reaction in the oxide layer, the NO_x composition reaches equilibrium at the interface leading to equal impedancemetric sensitivity to NO and NO_2. In addition, the sensor attached with the Pt/$ZnCr_2O_4$ double-layer as an sensing electrode showed high selectivity to NO_x because of the high catalytic activity of the Pt layer for oxidation of various reducing gases such as CO, H_2, CH_4 and C_3H_8 (Figure 14C and 15D)

[**Figure 13**] [Figure 14]

Although the sensors discussed above show promising results for high temperature NO_x detection, the effect of O_2 concentration change on the sensing performance was not investigated. To reduce oxygen dependence of NO_x sensors, Martin et al. fabricated an impedancemetric NO_x sensor with a planar YSZ electrolyte and two identical YSZ/Cr_2O_3 composite electrodes. [151] It was found that both the modulus |Z| and phase angle Θ of the sensor showed responses to the change of NO_x concentration, when a sinusoidal ac signal applied between the two electrodes. Θ appears to be more stable and shows a higher sensitivity to NO_x than the modulus |Z|. Phase angle Θ measured at low frequency of 10 Hz is sensitive to both the NO_x and O_2, while at higher frequencies of 1000 Hz, Θ is only sensitive to O_2. By using dual frequency measurement, the response of sensor in fluctuating O_2 background (2-18.9%) at low frequency can be adjusted by compensation from the response at high

frequency (except 2.0%), based on an algebraic relationship between the measured Θ at the two frequencies. The result of NO_x detection in varied O_2 concentration after compensation is shown in Figure 15. Excellent sensor performance is obtained for NO_x concentrations in the range of 8–50 ppm in background. The detail sensing mechanism was not provided in this work. In order to better understand the sensing mechanism, Woo et al. used a model electrochemical cell [Au/YSZ/Au] to isolate the role of the Au/porous YSZ interface [34], and used another cell [metal/YSZ porous/YSZ dense/YSZ porous /metal] (metal=Au, Pt, and Ag) to further investigate the role of the dense Au electrode [152]. It was suggested that the rate-determining step for NO-sensing may depend on the diffusion and adsorption of O_2; however the exact sensing mechanism was not determined. Woo et al. also designed an asymmetric cell design utilizing porous YSZ as electrolyte and Sr-doped lanthanum manganite (LSM) as electrode for impedance-based NO_x detection. [27] A virtual identical sensitivity toward NO and NO_2 was obtained at 575 ^oC, indicating that the equilibrium gas concentration was measured by the sensing electrode. Moreover, several other electrode materials were investigated as candidates applied in impedancemetric NO_x sensor, including Au wire [153], NiO [154], $NiCr_2O_4$ [155], $LaCr_{0.95}Mg_{0.05}O_3$ [156] and $La_{0.75}Sr_{0.25}Cr_{0.5}Mn_{0.5}O_{3-\delta}$ ($Ce_{0.9}Gd_{0.1}O_{1.95}$ as electrolyte) [157], as summarized in Table 4. All of these sensors are from laboratory tests and most of them operates around 600-700 ^oC. Recently, a prototype impendancemetric sensor using a dense gold sensing electrode, porous YSZ electrolyte, and a platinum counter electrode (Au/YSZ/Pt) were evaluated for measuring NO_x in diesel exhaust. [158] Phase angle was used as the response signal. The experimental sensor showed very good measurement capability for NO in the range of 25–250 ppm, with a response paralleling that of the FTIR and commercial sensor. The prototype sensor showed better sensitivity to NO_x at the lower concentration ranges. However, O_2 is an interferent for the experimental sensor, resulting in decreased sensitivity for NO_x measurement.

[Figure 15]

In conclusion, fabrication of highly selective impedancemetric NO_x sensors remains a challenge due to the potential interference from O_2 concentration variation in the gas sample. In addition, the electronics and signal processing equipment are more complicated than those of conventional sensors. Therefore, there are still numerous challenges which need to be overcome prior to the commercialization of impedancemetric sensors for gas detection in high temperature environments.

[Table 4]

4. Challenges of Solid-State Gas Sensor for High Temperature Application

The analysis of the three S's—stability, sensitivity and selectivity—is essential in any discussion of chemical sensor development. When dealing with harsh operation environments, especially high temperatures (above 600 ^{o}C), the thermal and long-term stability of the sensor devices are the prominent issue, along with the electrodes, electrolyte, sensing materials and substrates. The stability of a sensor is paramount to obtain accurate and reliable response, which is challenging at elevated temperatures. Regarding the electrodes, the rapid recrystallization rate of gold electrodes at high temperature, especially the nano- or micron-sized interdigitated gold electrodes, can change the geometry and morphology of the electrodes, thus leading to unstable response in long-term operation. The substitution of oxide electrodes offers promise in improving the long-term stability of these sensors.[159] Along with the development of nanoscience and nanotechnology, there is an increased amount of sensors based on nano-structured materials, mainly at low or mild temperature below 500 ^{o}C. The reason behind this is the ultrahigh surface to volume ratio which makes the sensor extremely sensitive to surface adsorbed gaseous species. However, most of current high temperature gas sensors are fabricated based on thin or thick film technologies and only a very few reports utilize nanostructured materials as sensing elements. One reason is that the morphological and structural stability of nanomaterials at high temperature is much more challenging than that of bulk material, since the reduction of surface area is a spontaneous process. There are only a few simple oxides, Ga_2O_3, CeO_2 and TiO_2 which may maintain their micro-morphology and chemical structure at high temperature above 800 ^{o}C. Perovskite oxide, generally ABO_3, is a group of thermal stable materials which are extremely suitable for high temperature applications. The perovskite structure can stabilize the transition metal oxides and usually have high melting and decomposition temperatures which can provide good thermal stability even for nano-structured materials. As an example, Figure 16 exhibits the thermal stability study of CeO_2 nanofibers[85] and perovskite $La_{0.67}Sr_{0.33}MnO_3$ nanofibers.[160] Both of the nanofibers samples were calcined at 1000 ^{o}C in air for 5 hours and naturally cooled down to room temperature with the process repeating 3 times. XRD and SEM characterization (Figure 16) indicates that before and after the thermal treatment (up to 1000 ^{o}C), both nanofibers maintain their chemical compositions and nanofibrous morphologies, indicating that good thermal stability can be

achieved for nanostructured materials if materials with proper thermal stability are carefully selected and designed. Another reason hindering the application of nanostructured materials for high temperature sensor application is the design of sensor configuration and fabrication. Most of gas sensors employing nanomaterials are resistor-type sensor based on semiconductors at mild temperature. Nanomaterial as sensing element can be easily cast or deposited on Pt or Au interdigitated electrode to complete the sensor fabrication. As discussed above, for resistive sensors, both nanostructured sensing material and electrode suffer a lot from instability at high temperature. For mixed potential sensors, nanomaterials with ultra-high surface area should be expected to enhance the sensitivity by providing more three-phase boundary sites. However, nanostructured sensing electrode could face several challenges, including the nanomaterial adhesion, mechanical properties and the connection of SE to measuring instrument. In addition, the sensing performance of mixed potential sensor strongly depends on the catalytic properties at and/or near the TPB line of nanostructured electrode/electrolyte/gas which can be easily influenced by sintering effects at high temperature, leading to amplified characteristic signal drift. Therefore, to employ nanotechnology in the design and development of gas sensors for high temperature application is still highly challenging.

[**Figure 16**]

Beyond the avenue of using nanostructured materials for improved sensitivity, a list of materials has also been screened for different gas detection to achieve good sensitivity. Perovskite oxides, as a group of thermal stable material, are investigated extensively for improved sensitivity and enhanced selectivity of the sensor. The perovskite structure has two differently-sized cations which makes it amenable to a variety of dopant additions. This doping flexibility allows for control of the transport and catalytic properties to optimize sensor performance.[161] The sensing performance of perovskite oxides towards different targets can be found in Tables 2-4. Besides the intrinsic electrochemical properties of materials, the preparation methods and fabrication process can affect sensor sensitivity, such as material thickness, porosity and sintering temperature etc. Each parameter needs to be optimized for best sensing performance.

Besides the thermal stability and sensitivity of sensing materials, selectivity remains the major challenge for all types of emission gas sensors, which is even more challenging in a harsh industrial

environment (e.g., high temperature, high pressure, complicated contaminants and dynamic gas flow). There are many concepts and on-going research which aim to improve the selectivity of high temperature gas sensors, which means these sensors are required to be able to detect low concentration of a specified analyte in other interfering gases. A spectrum of simple metal oxides, perovskite oxides, metal/metal oxide composites and oxide/oxide composites were intensively investigated. Some of them showed considerable selectivity to a specific target (e.g., $ZnCo_2O_4$ for selective C_3H_8 detection as discussed previously). [111] P-type and n-type semiconductors usually have opposite response directions towards reducing or oxidizing gases. Resistor-type sensor based on p-n heterojunction/mixtures with different p-n ratio ranging from p-type dominating to n-type dominating mixtures will show the sensing behavior transforming from p-type to n-type. At a specific ratio the sensor may only respond to a specific gas and the response towards other gases may cancel out, thus achieving good selectivity. A good example of this concept is the resistive CO sensor fabricated by n-anatase and p-rutile mixture which exhibited good selectivity to CO over CH_4, as discussed before. [88] This concept can be further explored for other p-type and n-type materials combinations. In addition to novel sensing materials, sensor configurations and sensing technologies are also important for improving selectivity. Adding a catalytic/physical filter layer to a sensor is a promising approach to obtain selectivity from the configuration aspect. As mentioned, a Pt catalytic layer which can promote oxidation of reducing gas (CO, H_2, CH_4 and C_3H_8) was added to the top of a $ZnCr_2O_4$ sensing electrode and resulted in high NO_x selectivity. [131] Besides, zeolites are another type of filter layer which has been employed to improve the selectivity in a number of sensors, including amperometric NO_x sensor[162], potentiometric NO_x sensor[163] and impedancemetric hydrocarbon sensor[37]. Different types of zeolite can be applied to achieve specific selectivity due to its catalytic and/or adsorbing properties. For example, if such sensors are covered with platinum exchanged Na-ZSM-5 zeolites, they become highly selective towards some saturated hydrocarbons. As shown in Figure 17, the impedancemetric gas sensors can selectively detect hydrocarbons using a Na-ZSM-5 zeolite film.[36] However, zeolite usually can only stand with a temperature up to 600 ^oC. The future study in new molecular sieving materials with super thermal stability could benefit the development of highly selective high temperature has sensors. Furthermore, a novel technique, so called high frequency impedancemetric measurement, has been recently applied to a Pt decorated CeO_2 nanofibers based sensor by our group. At high frequency, the impedance of the sensor to

oxidizing gas and weak reducing gas overlapped at 800 ^{o}C in Bode plot. By operating at high frequencies of 100 kHz, the sensor can selectively detect strong reducing gas (CO and C_3H_8) and eliminate the interference from NO, NO_2, SO_2 and CO_2 as shown in Figure 18. [164]

[**Figure 17**] [**Figure 18**]

5. Conclusions and Future Trends

High temperature gas sensors for harsh exhaust environments are of paramount importance to improve combustion efficiency and control emissions. Over past three decades, solid state oxide sensors for high temperature applications have been extensively studied with the goal to fabricate reliable, robust and cost-effective sensors possessing good sensitivity, selectivity and long-term stability. Generally, potentiometric gas sensors are characterized by high sensitivity and selectivity as well as long-term stability. Potentiometric oxygen sensors are the most successful and widely used sensors in automotive combustion process control nowadays. The future research should focus on the development of external reference-free potentiometric oxygen sensor with the reduced device size, which can provide the sensor more placement flexibility for more precise combustion control. Current research has demonstrated some external reference-free potentiometric oxygen sensors by using internal reference, such as metal/metal oxides system and only oxides as reference. However, the operation temperature of these sensors is around 600 ^{o}C which is far below the required high temperature for in-situ automotive application. Therefore, external reference-free potentiometric oxygen sensor, which can work at high temperature (800-1000 ^{o}C) with precise measurement and long-term stability, could be a future research direction. Resistive sensors can be an alternative for miniaturization purpose, due to their low cost, simple structure, easy fabrication and compatibility with electronic systems. A list of oxides has been investigated for either O_2 or combustibles CO/HCs detection in past several decades. However, for commercial success, major improvement in long-term stability, reliability, selectivity and temperature dependency of the sensors are required. One future topic of high temperature resistive sensors should be on the investigation of temperature-independent materials with high thermal stability and good sensitivity to target gas. Mixed potential gas sensors were extensively investigated to detect CO, HCs and NO_x. Due to the non-equilibrium sensing mechanism, most of these sensors operate in a temperature range of 500-600 ^{o}C. Only a few reported sensors can be operated over 700 ^{o}C. The operation window is limited by the fact that mixed

potential sensor should be operated in non-equilibrium conditions, which tend toward equilibrium with increasing reaction rates at high temperatures. To expand this window through the development of new electrode materials is another future research subject. Amperometric sensors, which can provide good sensitivity, usually suffer from poor thermal stability and the difficulty in designing a suitable diffusion barrier at high temperature. Also due to the complex sensor configuration, the reports on high temperature amperometric sensor are limited. Impedancemetric gas sensors are a relatively new and less developed type of sensor for high temperature application. Compared to conventional current or voltage measurements, it can provide more accurate measurement for low concentration of analyte (a few ppm). However, the auxiliary electronics and signal processing equipment create a more complicated system. In addition, the mechanisms of most impedancemetric sensors are poorly understood. With more efforts in fundamental studies and better understanding of sensing mechanism, impedancemetric technology could be better utilized to achieve the requirements of high temperature gas sensors in the future.

To conclude, although high temperature gas sensors encounter many challenges, the development of solid-state gas sensors is expected to continue and the market appears to be promising. There are two overall future research trends for developing solid-state high temperature gas sensors: 1) increased efforts in fundamental studies for better understanding of sensing mechanisms and the relation between sensing element and sensing properties. Most of the materials used as sensing elements have so far been developed empirically. The structure and properties of these materials should be characterized carefully and modeling and simulation can be involved to establish guidelines for the design of the sensor and develop reliable criteria for predicting and identifying the most useful materials for individual applications; and 2) New or improved materials synthesis, novel sensor designs, combination of sensing technologies and advanced device fabrication techniques are required to improve the stability and selectivity of the solid-state gas sensors. Due to the limit information and understanding of fundamentals in materials structure-property-function relationship, the screening of sensing materials in the past is basically on a basis of trial-and-error, which is lack of systematic study and cannot generate a full picture. Therefore, between the two future research trends, we prioritize the first one because materials simulation it is barely employed in the design/selection of high temperature sensing materials in the past three decades. With the establishment of more and more accurate materials models to reveal the structure-property-function

relationship, a computation method to simulate the response of various functional materials or composites to different targeted gases at high temperature is expected to play a critical role in the screening/selection of specific materials for specific gas in the design of high temperature gas sensor.

As selectivity is the major challenge for all types of high temperature gas sensors, developing selective high temperature gas sensors requires increased research efforts. Novel strategies such as building sensor arrays, using bi-modular detection mode, polarizing the sensing electrode at different voltages or current, and/or employing physical/catalytic filter layers, should be explored. In addition, the combination of multiple strategies is also necessary to achieve excellent sensing performance with good stability, high sensitivity and selectivity.

6. Acknowledgements

We greatly appreciate the funding from NSF and DOE.

7. References

1. D. D. Lee and D. S. Lee, *Ieee Sensors Journal*, 2001, **1**, 214-224.
2. R. Mukundan and F. Garzon, *The Electrochemical Society Interface*, 2004, **Summer**, 30-35.
3. S. Akbar, P. Dutta and C. H. Lee, *Int. J. Appl. Ceram. Technol.*, 2006, **3**, 302-311.
4. J. Kaspar, P. Fornasiero and N. Hickey, *Catalysis Today*, 2003, **77**, 419-449.
5. J. Riegel, H. Neumann and H. M. Wiedenmann, *Solid State Ion.*, 2002, **152**, 783-800.
6. N. Docquier and S. Candel, *Progress in Energy and Combustion Science*, 2002, **28**, 107-150.
7. C. O. Park, S. A. Akbar and W. Weppner, *Journal of Materials Science*, 2003, **38**, 4639-4660.
8. W. Weppner, *Sensors and Actuators*, 1987, **12**, 107-119.
9. C. O. Park, J. W. Fergus, N. Miura, J. Park and A. Choi, *Ionics*, 2009, **15**, 261-284.
10. M. Gauthier and A. Chamberland, *J. Electrochem. Soc.*, 1977, **124**, 1579-1583.
11. W. L. Worrell and Q. G. Liu, *Journal of Electroanalytical Chemistry*, 1984, **168**, 355-362.
12. L. Wang and R. V. Kumar, *Sens. Actuator B-Chem.*, 2003, **88**, 292-299.
13. G. M. Kale, L. Wang, J. E. Hayes, J. Congjin and Y. R. Hong, *Journal of Materials Science*, 2003, **38**, 4293-4300.
14. H. Kurosawa, Y. T. Yan, N. Miura and N. Yamazoe, *Solid State Ion.*, 1995, **79**, 338-343.
15. L. Wang and R. V. Kumar, *Journal of Applied Electrochemistry*, 2006, **36**, 173-178.
16. P. Pasierb and M. Rekas, *Journal of Solid State Electrochemistry*, 2009, **13**, 3-25.
17. J. W. Fergus, *Journal of Solid State Electrochemistry*, 2011, **15**, 971-984.
18. E. L. Brosha, R. Mukundan, D. R. Brown, F. H. Garzon and J. H. Visser, *Solid State Ion.*, 2002, **148**, 61-69.
19. L. Chevallier, E. Di Bartolomeo, M. L. Grilli, M. Mainas, B. White, E. D. Wachsman and E. Travers, *Sens. Actuator B-Chem.*, 2008, **129**, 591-598.
20. E. Di Bartolomeo, N. Kaabbuathong, M. L. Grilli and E. Traversa, *Solid State Ion.*, 2004, **171**, 173-181.
21. N. Miura, M. Nakatou and S. Zhuiykov, *Ceram. Int.*, 2004, **30**, 1135-1139.
22. J. Zosel, K. Ahlborn, R. Muller, D. Westphal, V. Vashook and U. Guth, *Solid State Ion.*, 2004, **169**, 115-119.
23. J. R. Stetter and J. Li, *Chem. Rev.*, 2008, **108**, 352-366.
24. R. Ramamoorthy, P. K. Dutta and S. A. Akbar, *Journal of Materials Science*, 2003, **38**, 4271-4282.
25. C. O. Park and S. A. Akbar, *Journal of Materials Science*, 2003, **38**, 4611-4637.
26. J. R. Macdonald, ed., *Impedance Spectroscopy: Emphasizing Solid Materials and Systems*, John Wiley & Sons, New York, 1987.
27. L. Y. Woo, R. S. Glass, R. F. Novak and J. H. Visser, *J. Electrochem. Soc.*, 2010, **157**, J81-J87.
28. N. Miura, M. Nakatou and S. Zhuiykov, *Sens. Actuator B-Chem.*, 2003, **93**, 221-228.
29. M. Nakatou and N. Miura, *Electrochem. Commun.*, 2004, **6**, 995-998.
30. M. Nakatou and N. Miura, *Solid State Ion.*, 2005, **176**, 2511-2515.
31. R. Wama, M. Utiyama, V. V. Plashnitsa and N. Miura, *Electrochem. Commun.*, 2007, **9**, 2774-2777.
32. R. Wama, V. V. Plashnitsa, P. Elumalai, M. Utiyama and N. Miura, *Solid State Ion.*, 2010, **181**, 359-363.
33. K. I. Shimizu, K. Kashiwagi, H. Nishiyama, S. Kakimoto, S. Sugaya, H. Yokoi and A. Satsuma, *Sens. Actuator B-Chem.*, 2008, **130**, 707-712.

34. L. Y. Woo, L. P. Martin, R. S. Glass and R. J. Gorte, *J. Electrochem. Soc.*, 2007, **154**, J129-J135.
35. N. Q. Wu, Z. Chen, J. H. Xu, M. Chyu and S. X. Mao, *Sens. Actuator B-Chem.*, 2005, **110**, 49-53.
36. G. Hagen, A. Dubbe, G. Fischerauer and R. Moos, *Sens. Actuator B-Chem.*, 2006, **118**, 73-77.
37. G. Hagen, A. Dubbe, F. Rettig, A. Jerger, T. Birkhofer, R. Muller, C. Plog and R. Moos, *Sens. Actuator B-Chem.*, 2006, **119**, 441-448.
38. S. Colominas, J. Abella and L. Victori, *J. Nucl. Mater.*, 2004, **335**, 260-263.
39. S. Colominas and J. Abella, *Sens. Actuator B-Chem.*, 2010, **145**, 720-725.
40. J. V. Spirig, R. Ramamoorthy, S. A. Akbar, J. L. Routbort, D. Singh and P. K. Dutta, *Sens. Actuator B-Chem.*, 2007, **124**, 192-201.
41. H. Kaneko, T. Okamura, H. Taimatsu, Y. Matsuki and H. Nishida, *Sens. Actuator B-Chem.*, 2005, **108**, 331-334.
42. H. Kaneko, T. Okamura and H. Taimatsu, *Sens. Actuator B-Chem.*, 2003, **93**, 205-208.
43. A. Chowdhury, S. A. Akbar, S. Kapileshwar and J. R. Schorr, *J. Electrochem. Soc.*, 2001, **148**, G91-G94.
44. Q. Hu, T. Jacobsen, K. V. Hansen and M. Mogensen, *J. Electrochem. Soc.*, 2012, **159**, B811-B817.
45. N. Rajabbeigi, B. Elyassi, A. Khodadadi, S. S. Mohajerzadeh and M. Sahimi, *Sens. Actuator B-Chem.*, 2004, **100**, 139-142.
46. B. Elyassi, N. Rajabbeigi, A. Khodadadi, S. S. Mohajerzadeh and M. Sahimi, *Sens. Actuator B-Chem.*, 2004, **103**, 178-183.
47. N. Rajabbeigi, B. Elyassi, A. A. Khodadadi, S. Mohajerzadeh, Y. Mortazavi and M. Sahimi, *Sens. Actuator B-Chem.*, 2005, **108**, 341-345.
48. N. Miura, H. Jin, R. Wama, S. Nakakubo, P. Elumalai and V. V. Plashnitsa, *Sens. Actuator B-Chem.*, 2011, **152**, 261-266.
49. W. Gopel, G. Reinhardt and M. Rosch, *Solid State Ion.*, 2000, **136**, 519-531.
50. M. Schulz, D. Richter, J. Sauerwald and H. Fritze, *Integrated Ferroelectrics*, 2010, **115**, 41-56.
51. V. Thangadurai and W. Weppner, *Electrochim. Acta*, 2004, **49**, 1577-1585.
52. J. X. Han, F. Zhou, J. X. Bao, X. J. Wang and X. W. Song, *Electrochim. Acta*, 2013, **108**, 763-768.
53. M. Benammar, *Measurement Science & Technology*, 1994, **5**, 757-767.
54. E. M. Logothetis, J. H. Visser, R. E. Soltis and L. Rimai, *Sens. Actuator B-Chem.*, 1992, **9**, 183-189.
55. Y. L. Xu, X. H. Zhou and O. T. Sorensen, *Sens. Actuator B-Chem.*, 2000, **65**, 2-4.
56. M. Q. Li and Y. F. Chen, *Sens. Actuator B-Chem.*, 1996, **32**, 83-85.
57. M. Bartic, C. I. Baban, H. Suzuki, M. Ogita and M. Isai, *Journal of the American Ceramic Society*, 2007, **90**, 2879-2884.
58. F. Millot and P. Demierry, *Journal of Physics and Chemistry of Solids*, 1985, **46**, 797-801.
59. N. Izu, N. Oh-hori, M. Itou, W. Shin, I. Matsubara and N. Murayama, *Sens. Actuator B-Chem.*, 2005, **108**, 238-243.
60. M. Kamiya, E. Shimada, Y. Ikuma, M. Komatsu and H. Haneda, *J. Electrochem. Soc.*, 2000, **147**, 1222-1227.
61. E. B. Varhegyi, I. V. Perczel, J. Gerblinger, M. Fleischer, H. Meixner and J. Giber, *Sens. Actuator B-Chem.*, 1994, **19**, 569-572.
62. W. Menesklou, H. J. Schreiner, K. H. Hardtl and E. Ivers-Tiffee, *Sens. Actuator B-Chem.*, 1999, **59**, 184-189.
63. N. Izu, W. Shin, I. Matsubara and N. Murayama, *Sens. Actuator B-Chem.*, 2004, **101**, 381-386.
64. N. Izu, W. Shin, I. Matsubara, N. Murayama, N. Oh-hori and M. Itou, *Sens. Actuator B-Chem.*, 2005,

108, 216-222.
65. N. Izu, S. Nishizaki, W. Shin, T. Itoh, M. Nishibori and I. Matsubara, *Sensors*, 2009, **9**, 8884-8895.
66. C. Y. Chen and K. H. Chang, *Sens. Actuator B-Chem.*, 2012, **162**, 68-75.
67. A. Rothschild and H. L. Tuller, *J. Electroceram.*, 2006, **17**, 1005-1012.
68. A. Rothschild, S. J. Litzelman, H. L. Tuller, W. Menesklou, T. Schneider and E. Ivers-Tiffee, *Sens. Actuator B-Chem.*, 2005, **108**, 223-230.
69. G. Neri, A. Bonavita, G. Micali, G. Rizzo, R. Licheri, R. Orru and G. Cao, *Sens. Actuator B-Chem.*, 2007, **126**, 258-265.
70. G. Neri, G. Micali, A. Bonavita, R. Licheri, R. Orru, G. Cao, D. Marzorati, E. M. Borla, E. Roncari and A. Sanson, *Sens. Actuator B-Chem.*, 2008, **134**, 647-653.
71. R. Moos, F. Rettig, A. Hurland and C. Plog, *Sens. Actuator B-Chem.*, 2003, **93**, 43-50.
72. K. Sahner, R. Moos, N. Izu, W. Shin and N. Murayama, *Sens. Actuator B-Chem.*, 2006, **113**, 112-119.
73. R. Moos, W. Menesklou, H. J. Schreiner and K. H. Hardtl, *Sens. Actuator B-Chem.*, 2000, **67**, 178-183.
74. F. Rettig, R. Moos and C. Plog, *J. Electroceram.*, 2004, **13**, 733-738.
75. M. Bektas, D. Schonauer-Kamin, G. Hagen, A. Mergner, C. Bojer, S. Lippert, W. Milius, J. Breu and R. Moos, *Sens. Actuator B-Chem.*, 2014, **190**, 208-213.
76. K. Sahner, J. Straub and R. Moos, *J. Electroceram.*, 2006, **16**, 179-186.
77. R. Moos, *Int. J. Appl. Ceram. Technol.*, 2005, **2**, 401-413.
78. M. Fleischer and H. Meixner, *Journal of Vacuum Science & Technology a-Vacuum Surfaces and Films*, 1999, **17**, 1866-1872.
79. U. Hoefer, J. Frank and M. Fleischer, *Sens. Actuator B-Chem.*, 2001, **78**, 6-11.
80. G. Eranna, B. C. Joshi, D. P. Runthala and R. P. Gupta, *Critical Reviews in Solid State and Materials Sciences*, 2004, **29**, 111-188.
81. M. Fleischer and H. Meixner, *Sens. Actuator B-Chem.*, 1997, **43**, 1-10.
82. J. Frank, M. Fleischer and H. Meixner, *Sens. Actuator B-Chem.*, 1998, **48**, 318-321.
83. T. Schwebel, M. Fleischer, H. Meixner and C. D. Kohl, *Sens. Actuator B-Chem.*, 1998, **49**, 46-51.
84. A. C. Lang, M. Fleischer and H. Meixner, *Sens. Actuator B-Chem.*, 2000, **66**, 80-84.
85. Y. X. Liu, Y. Ding, L. C. Zhang, P. X. Gao and Y. Lei, *Rsc Advances*, 2012, **2**, 5193-5198.
86. P. K. Dutta, A. Ginwalla, B. Hogg, B. R. Patton, B. Chwieroth, Z. Liang, P. Gouma, M. Mills and S. Akbar, *J. Phys. Chem. B*, 1999, **103**, 4412-4422.
87. N. O. Savage, S. A. Akbar and P. K. Dutta, *Sens. Actuator B-Chem.*, 2001, **72**, 239-248.
88. N. Savage, B. Chwieroth, A. Ginwalla, B. R. Patton, S. A. Akbar and P. K. Dutta, *Sens. Actuator B-Chem.*, 2001, **79**, 17-27.
89. X. G. Li, R. Ramasamy and P. K. Dutta, *Sens. Actuator B-Chem.*, 2009, **143**, 308-315.
90. J. Trimboli and P. K. Dutta, *Sens. Actuator B-Chem.*, 2004, **102**, 132-141.
91. N. Guillet, R. Lalauze and C. Pijolat, *Sens. Actuator B-Chem.*, 2004, **98**, 130-139.
92. R. Mukundan, E. L. Brosha, D. R. Brown and F. H. Garzon, *Electrochem. Solid State Lett.*, 1999, **2**, 412-414.
93. R. Mukundan, E. L. Brosha, D. R. Brown and F. H. Garzon, *J. Electrochem. Soc.*, 2000, **147**, 1583-1588.
94. J. W. Fergus, *Sens. Actuator B-Chem.*, 2007, **122**, 683-693.
95. E. Di Bartolomeo and M. L. Grilli, *J. Eur. Ceram. Soc.*, 2005, **25**, 2959-2964.
96. A. Dutta, N. Kaabbuathong, M. L. Grilli, E. Di Bartolomeo and E. Traversa, *J. Electrochem. Soc.*,

2003, **150**, H33-H37.
97. L. Chevallier, E. Di Bartolomeo, M. L. Grilli and E. Traversa, *Sens. Actuator B-Chem.*, 2008, **130**, 514-519.
98. L. Chevallier, S. Cordiner, E. Traversa and E. Di Bartolomeo, *J. Electrochem. Soc.*, 2009, **156**, J12-J15.
99. L. Chevallier, E. Traversa and E. Di Bartolomeo, *J. Electrochem. Soc.*, 2010, **157**, J386-J391.
100. J. Zosel, D. Westphal, S. Jakobs, R. Muller and U. Guth, *Solid State Ion.*, 2002, **152**, 525-529.
101. U. Guth and J. Zosel, *Ionics*, 2004, **10**, 366-377.
102. J. Zosel, R. Miller, V. Vashook and U. Guth, *Solid State Ion.*, 2004, **175**, 531-533.
103. X. G. Li and G. M. Kale, *Sens. Actuator B-Chem.*, 2006, **120**, 150-155.
104. X. G. Li and G. M. Kale, *Sens. Actuator B-Chem.*, 2007, **123**, 254-261.
105. G. M. Kale, *Adv. Powder Technol.*, 2009, **20**, 426-431.
106. E. L. Brosha, R. Mukundan, D. R. Brown, F. H. Garzon, J. H. Visser, M. Zanini, Z. Zhou and E. M. Logothetis, *Sens. Actuator B-Chem.*, 2000, **69**, 171-182.
107. E. L. Brosha, R. Mukundan, D. R. Brown and F. H. Garzon, *Sens. Actuator B-Chem.*, 2002, **87**, 47-57.
108. E. L. Brosha, R. Mukundan, R. Lujan and F. H. Garzon, *Sens. Actuator B-Chem.*, 2006, **119**, 398-408.
109. N. Miura, T. Shiraishi, K. Shimanoe and N. Yamazoe, *Electrochem. Commun.*, 2000, **2**, 77-80.
110. P. Elumalai, V. V. Plashnitsa, Y. Fujio and N. Miura, *Sens. Actuator B-Chem.*, 2010, **144**, 215-219.
111. F. J. Sun, X. G. Li, L. P. Liu and J. Wang, *Sens. Actuator B-Chem.*, 2013, **184**, 220-227.
112. T. Inaba, K. Saji and J. Sakata, *Sens. Actuator B-Chem.*, 2005, **108**, 374-378.
113. D. Eskilsson, M. Ronnback, J. Samuelsson and C. Tullin, *Biomass & Bioenergy*, 2004, **27**, 541-546.
114. J. W. Fergus, *Sens. Actuator B-Chem.*, 2007, **121**, 652-663.
115. N. Miura, G. Y. Lu and N. Yamazoe, *Sens. Actuator B-Chem.*, 1998, **52**, 169-178.
116. N. Miura, G. Lu, M. Ono and N. Yamazoe, *Solid State Ion.*, 1999, **117**, 283-290.
117. A. Dutta and T. Ishihara, *Electrochem. Solid State Lett.*, 2005, **8**, H46-H48.
118. A. Dutta and T. Ishihara, *Sens. Actuator B-Chem.*, 2005, **108**, 309-313.
119. A. Dutta and T. Ishihara, *Mater. Manuf. Process.*, 2006, **21**, 225-228.
120. T. Ueda, T. Nagano, H. Okawa and S. Takahashi, *Electrochem. Commun.*, 2009, **11**, 1654-1656.
121. T. Ueda, M. Umeda, H. Okawa and S. Takahashi, *Ionics*, 2012, **18**, 337-342.
122. P. Schmidt-Zhang, W. Zhang, F. Gerlach, A. Ahlborn and U. Guth, *Sens. Actuator B-Chem.*, 2005, **108**, 797-802.
123. L. Wang, Y. F. Wang, L. Dai, Y. H. Li, J. Zhu and H. Z. Zhou, *J. Alloy. Compd.*, 2014, **583**, 361-365.
124. L. E. Depero, M. Ferroni, V. Guidi, G. Marca, G. Martinelli, P. Nelli, L. Sangaletti and G. Sberveglieri, *Sensors and Actuators B: Chemical*, 1996, **36**, 381-383.
125. M. Ferroni, V. Guidi, G. Martinelli, P. Nelli and G. Sberveglieri, *Sens. Actuator B-Chem.*, 1997, **44**, 499-502.
126. S. Zhuiykov and N. Miura, *Sens. Actuator B-Chem.*, 2007, **121**, 639-651.
127. G. Lu, N. Miura and N. Yamazoe, *Sens. Actuator B-Chem.*, 2000, **65**, 125-127.
128. S. Zhuiykov, T. Nakano, A. Kunimoto, N. Yamazoe and N. Miura, *Electrochem. Commun.*, 2001, **3**, 97-101.
129. N. Miura, S. Zhuiykov, T. Ono, M. Hasei and N. Yamazoe, *Sens. Actuator B-Chem.*, 2002, **83**, 222-229.
130. S. Zhuiykov, T. Ono, N. Yamazoe and N. Miura, *Solid State Ion.*, 2002, **152**, 801-807.
131. N. Miura, T. Koga, M. Nakatou, P. Elumalai and M. Hasei, *J. Electroceram.*, 2006, **17**, 979-986.

132. N. Miura, K. Akisada, J. Wang, S. Zhuiykov and T. Ono, *Ionics*, 2004, **10**, 1-9.
133. P. Elumalai and N. Miura, *Solid State Ion.*, 2005, **176**, 2517-2522.
134. P. Elumalai, J. Wang, S. Zhuiykov, D. Terada, M. Hasei and N. Miura, *J. Electrochem. Soc.*, 2005, **152**, H95-H101.
135. N. Miura, J. Wang, M. Nakatou, P. Elumalai, S. Zhuiykov and M. Hasei, *Sens. Actuator B-Chem.*, 2006, **114**, 903-909.
136. N. Miura, J. Wang, M. Nakatou, P. Elumalai and M. Hasei, *Electrochem. Solid State Lett.*, 2005, **8**, H9-H11.
137. V. V. Plashnitsa, T. Ueda, P. Elumalai and N. Miura, *Sens. Actuator B-Chem.*, 2008, **130**, 231-239.
138. P. Elumalai, V. V. Plashnitsa, T. Ueda, M. Hasei and N. Miura, *Ionics*, 2007, **13**, 387-393.
139. K. Mahendraprabhu, N. Miura and P. Elumalai, *Ionics*, 2013, **19**, 1681-1686.
140. J. Wang, P. Elumalai, D. Terada, M. Hasei and N. Miura, *Solid State Ion.*, 2006, **177**, 2305-2311.
141. V. V. Plashnitsa, T. Ueda and N. Miura, *Int. J. Appl. Ceram. Technol.*, 2006, **3**, 127-133.
142. N. Miura, J. A. Wang, P. Elumalai, T. Ueda, D. Terada and M. Hasei, *J. Electrochem. Soc.*, 2007, **154**, J246-J252.
143. P. Elumalai, V. V. Plashnitsa, T. Ueda and N. Miura, *Electrochem. Commun.*, 2008, **10**, 745-748.
144. P. Elumalai, J. Zosel, U. Guth and N. Miura, *Ionics*, 2009, **15**, 405-411.
145. P. Elumalai, V. V. Plashnitsa, Y. Fujio and N. Miura, *J. Electrochem. Soc.*, 2009, **156**, J288-J293.
146. C. Lopez-Gandara, J. M. Fernandez-Sanjuan, F. M. Ramos and A. Cirera, *Sens. Actuator B-Chem.*, 2012, **175**, 225-233.
147. X. S. Liang, S. Q. Yang, J. G. Li, H. Zhang, Q. Diao, W. Zhao and G. Y. Lu, *Sens. Actuator B-Chem.*, 2011, **158**, 1-8.
148. C. G. Yin, Y. Z. Guan, Z. Zhu, X. S. Liang, B. Wang, Q. Diao, H. Zhang, J. Ma, F. M. Liu, Y. F. Sun, J. Zheng and G. Y. Lu, *Sens. Actuator B-Chem.*, 2013, **183**, 474-477.
149. J. M. Rheaume and A. P. Pisano, *Ionics*, 2011, **17**, 99-108.
150. N. Miura, M. Nakatou and S. Zhuiykov, *Electrochem. Commun.*, 2002, **4**, 284-287.
151. L. P. Martin, L. Y. Woo and R. S. Glass, *J. Electrochem. Soc.*, 2007, **154**, J97-J104.
152. L. Y. Woo, L. P. Martin, R. S. Glass, W. S. Wang, S. Jung, R. J. Gorte, E. P. Murray, R. F. Novak and J. H. Visser, *J. Electrochem. Soc.*, 2008, **155**, J32-J40.
153. J. M. Rheaume and A. P. Pisano, *Journal of Solid State Electrochemistry*, 2012, **16**, 3603-3610.
154. L. Wang, Z. C. Hao, L. Dai, Y. H. Li and H. Z. Zhou, *Materials Letters*, 2012, **87**, 24-27.
155. M. Stranzenbach, E. Gramckow and B. Saruhan, *Sens. Actuator B-Chem.*, 2007, **127**, 224-230.
156. Erica P. Murraya, Robert Novaka, David Kubinskia, Richard Soltisa, Jaco Vissera, Leta Woob, L. M. and and R. Glassb, *ECS Transactions*, 2008, **6**, 43-62.
157. L. Dai, L. Wang, B. J. Zhao, Y. H. Li, J. Zhu and Y. L. Wu, *Sens. Actuator B-Chem.*, 2013, **188**, 778-786.
158. L. Y. Woo, R. S. Glass, R. F. Novak and J. H. Visser, *Sens. Actuator B-Chem.*, 2011, **157**, 115-121.
159. F. H. Garzon, R. Mukundan and E. L. Brosha, *Solid State Ion.*, 2000, **136**, 633-638.
160. Y. X. Liu, Y. Ding, H. Y. Gao, L. C. Zhang, P. X. Gao, B. K. Li and Y. Lei, *Rsc Advances*, 2012, **2**, 3872-3877.
161. J. W. Fergus, *Sens. Actuator B-Chem.*, 2007, **123**, 1169-1179.
162. J. C. Yang and P. K. Dutta, *Sens. Actuator B-Chem.*, 2007, **123**, 929-936.
163. J. C. Yang and P. K. Dutta, *Sens. Actuator B-Chem.*, 2007, **125**, 30-39.
164. Y. Liu and Y. Lei, *Sensors and Actuators B: Chemical*, 2013, **188**, 1141-1147.

165. M. Fleischer, *Measurement Science & Technology*, 2008, **19**.
166. H. J. Beie and A. Gnorich, *Sens. Actuator B-Chem.*, 1991, **4**, 393-399.
167. N. Izu, W. Shin, N. Murayarna and S. Kanzaki, *Sens. Actuator B-Chem.*, 2002, **87**, 95-98.
168. S. V. Manorama, N. Izu, W. Shin, I. Matsubara and N. Murayama, *Sens. Actuator B-Chem.*, 2003, **89**, 299-304.
169. M. Zhang, X. D. Wang, F. M. Wang and W. C. Li, *Sens. Actuator B-Chem.*, 2003, **92**, 167-170.
170. V. K. Josepovits, O. Krafcsik, G. Kiss and I. V. Perczel, *Sens. Actuator B-Chem.*, 1998, **48**, 373-375.
171. J. Frank, M. Fleischer and H. Meixner, *Sens. Actuator B-Chem.*, 1996, **34**, 373-377.
172. T. Schwebel, M. Fleischer and H. Meixner, *Sens. Actuator B-Chem.*, 2000, **65**, 176-180.
173. J. Z. Zhu, C. X. Ren, G. L. Chen, C. Y. Yu, J. L. Wu and H. C. Mu, *Sens. Actuator B-Chem.*, 1996, **32**, 209-213.
174. L. Y. Zheng, M. X. Xu and T. X. Xu, *Sens. Actuator B-Chem.*, 2000, **66**, 28-30.
175. R. K. Sharma, M. C. Bhatnagar and G. L. Sharma, *Sens. Actuator B-Chem.*, 1997, **45**, 209-215.
176. J. C. C. Abrantes, J. A. Labrincha and J. R. Frade, *Sens. Actuator B-Chem.*, 1999, **56**, 198-205.
177. U. Lampe, J. Gerblinger and H. Meixner, *Sens. Actuator B-Chem.*, 1995, **25**, 657-660.
178. D. Westphal, S. Jakobs and U. Guth, *Ionics*, 2001, **7**, 182-186.
179. L. Chevallier, M. L. Grilli, E. Di Bartolomeo and E. Traversa, *Int. J. Appl. Ceram. Technol.*, 2006, **3**, 393-400.
180. Q. Diao, C. G. Yin, Y. W. Liu, J. G. Li, X. Gong, X. S. Liang, S. Q. Yang, H. Chen and G. Y. Lu, *Sens. Actuator B-Chem.*, 2013, **180**, 90-95.

Figure Captions

Figure 1. (A) Schematic illustration of an internal reference oxygen sensor (IROS). It consists of an IRE, an electrolyte, an SE and a sealing layer. V_{cell} is the voltage between the IRE and the SE, which is used for pO_2 measurement. (B) Photo of two IROSes, both with foot print ca. 10 × 10 mm. (C) SEM image (Inlens) of the cross section of a polished cell. Reprinted with permission from Ref [44].

Figure 2. (A) Schematic views and photos for the fabricated planar-like rod-type YSZ-based sensors. (B) Response transients to various gases (100 ppm each) for the rod-type sensor using each of Pt- and Au-SEs (vs. Mn_2O_3-RE). (Au-SE was used for a comparison). Dependence of *emf* on the normalized A/F ratio (λ) for (C) conventional tubular YSZ-based sensors using inner Pt/air-RE and (D) rod-type sensors using Mn_2O_3-RE. Operation condition: 550 ^oC in the presence of 5 vol.% water vapor. Reprinted with permission from Ref [48]

Figure 3. (A) Structure diagram of a limiting current type oxygen sensor using $Ce_{0.8}Sm_{0.2}O_{1.9}$ (SDC) electrolyte and LSCF dense diffusion barrier. (B) Sensor responses at various temperatures. Reprinted with permission from Ref [52]

Figure 4. (A) Interdigital structure electrodes used for sensor characterizations of (a) OMM and (b) OMM and TCM combination. (B) Outputs of the resistive oxygen sensors with TCM in a temperature range of 923-1123 K with oxygen partial pressures of 1.0 atm and 0.01 atm. The applied voltage was 30 V. (C) Dynamic response of the sensor sensitivity to change in oxygen pressure at 1123 K and 1073 K. Reprinted with permission from Ref [66]

Figure 5. Conductivity as a function of oxygen pressure at different temperatures and STF compositions. STF01 = $SrTi_{0.99}Fe_{0.01}O_{3-\delta}$, STF35 = $SrTi_{0.65}Fe_{0.35}O_{3-\delta}$, SF = $SrFeO_{3-\delta}$. Reprinted with permission from Ref [68]

Figure 6. Models of the three regimes of gas reaction of simple oxide semiconductors. Reprinted with permission from Ref. [165].

Figure 7. (A) Typical responses of CeO_2 nanofibers-based sensor upon periodic exposure to different concentrations of carbon monoxide at an applied DC bias of 1 V at 800 ^oC and 1000 ^oC. (B) Calibration curves for CO response of CeO_2 nanofibers-based sensor at an applied DC bias of 1 V at 800 ^oC and 1000 ^oC. Inset is the SEM image of electrospun CeO_2 nanofibers after calcination at 1000 ^oC. Reprinted with permission from Ref [85]

Figure 8. (A) Cross sensitivities to various gases (400 ppm each) for the YSZ-based sensors using (a) Au-SE, (b) NiO-SE and (c) NiO (+5 wt% Au)-SE operating at 600 ^{o}C under the wet condition (5 vol% H_2O + 5 vol% O_2). Reprinted with permission from Ref. [110]. (B) Comparison of the sensitivities of the sensor using (A) Zn–Sn–O composite sensing electrode and (C) the $ZnCo_2O_4$ sensing electrode to CO, C_3H_8 and NO_2 at 600 ^{o}C. Reprinted with permission from Ref. [111]

Figure 9. (A) Potential of Pt and Pr_6O_{11} electrodes at 800 ^{o}C with respect to reference electrode. (B) Output of gas-detection cell when C_3H_8, CH_4, H_2, and CO were injected in 22% O2 at 800 ^{o}C. (C) Experimental sensor output with and without pump being driven. Reprinted with permission from Ref. [112]

Figure 10. (A) The relationship between response currents and NO_2 concentrations at different temperatures. (B) Dependence of response to 300 ppm NO_2 at 500 ^{o}C on concentration of O_2 (0–10 vol.%) and CO_2 (0–10 vol.%), respectively. Inset shows the SEM image of the cross-section of YSZ porous layer GSF-impregnation. Reprinted with permission from Ref. [123]

Figure 11. (A) A histogram showing the sensing response (at 850 ^{o}C) of various oxide SEs to 400 ppm NO_2. Reprinted with permission from Ref. [136]. Comparison of sensitivity (Δemf) to 50 ppm NO_2 for the sensors using (B) NiO-SE loaded with various noble-metals and (C) NiO-SE added with various metal-oxide additives at 800 ^{o}C (base gas: 5 vol.% O_2 + 5 vol.% H_2O+N_2 balance). Reprinted with permission from Ref. [140][142] (D) Various processes occurring at NiO-SE and Co doped NiO-SE/YSZ layers. Reprinted with permission from Ref. [145].

Figure 12. (A) Schematic view of the planar mixed potential NO_2 sensor based on YSZ and NiO electrode. (B) The relationship between surface roughness and the used HF concentration. (C) The kinetic response of the sensor using YSZ treated with different HF concentration to 20–500 ppm NO_2. (D) Sensitivities of the sensor using the YSZ substrate that corroded by 40% HF to various gases at 850 ^{o}C. Reprinted with permission from Ref. [147]

Figure 13. (A) Complex impedance plots in the base air and the sample gas with each of various concentrations of (a) NO and (b) NO_2 at 700 ^{o}C for the YSZ-based device using $ZnCr_2O_4$ SE. (B) The probable equivalent circuit for the YSZ-based device using the $ZnCr_2O_4$ SE. Reprinted with permission from Ref. [28]

Figure 14. (A) Dependence of gas sensitivity ($|Z|_{air} - |Z|_{gas}$) on NO_x concentration at 700 ^{o}C for the impedancemetric device using the 39 μm-thick $ZnCr_2O_4$-SE. (B) Dependence of impedance value on composition ratio of NO_2 at 700 ^{o}C. The concentration of total NO_x was fixed at 400 ppm. (C) Configuration of tubular NO_x sensor using YSZ and $ZnCr_2O_4$ sensing electrode (SE). (D) Cross sensitivity to various gases (400 pm each) at 700 ^{o}C for the impedancemetric sensor attached with Pt/

$ZnCr_2O_4$-SE. Reprinted with permission from Ref. [131]

Figure 15. |Z| and Θ measured at (A) 10 Hz and (B) 1000 Hz at 600°C with an excitation voltage of 50 mV rms. The O_2 concentration varies from 2 to 18.9%, and NO_x exposures of 50, 25, 15, and 8 ppm of NO (1st) and NO_2 (2nd) are performed at each concentration. (C) Linear correlation between phase angles measured at 10 Hz vs 1000 Hz. (D) Sensor response, Θ (10 Hz) compensated for the O_2 background using Θ (1000 Hz) and the linear correlation. Reprinted with permission from Ref. [151]

Figure 16. (A) XRD patterns for the $CeO_{2(1000)}$ nanofibers, $CeO_{2(1000\times3)}$ nanofibers obtained after thermal stability study and the standard values for CeO_2. Insets show the SEM images of $CeO_{2(1000)}$ and $CeO_{2(1000\times3)}$. Reprinted with permission from Ref. [85]. (B) XRD patterns for the $LSMO_{(800)}$ nanofibers, $LSMO_{(1000)}$ nanofibers obtained after thermal stability study and the standard values for LSMO. Insets show the SEM images of $LSMO_{(800)}$ and $LSMO_{(1000)}$. Reprinted with permission from Ref. [160].

Figure 17. (A) Impedance spectra (Nyquist-plots) of a zeolite covered interdigitated electrode structure with an additional chromium oxide (d_{Cr2O3}=50 nm) film between gold electrode and zeolite film (d_{Cr}=100 nm; d_{Au}=400 nm). Measurement range from 20 Hz to 1 MHz. (B) Results of a zeolite covered interdigitated electrode structure on alumina substrate with additional chromium oxide layer (d_{Cr2O3}=100 nm). Measurement frequency=20 Hz. Reprinted with permission from Ref. [37]

Figure 18. (A) Impedance spectra (Bode-plots) of Pt-CeO_2 NFs based sensor in N_2 and different gases (O_2, CO, NO, CO_2 and SO_2 balanced by N_2) with varied concentrations. The inset shows the plots in the red dash box in large scale. (B) Summarized sensitivity/selectivity of the impedancemetric sensor and resistor-type sensor in different gases. (C) Real-time selectivity study on resistor-type Pt-CeO_2 NFs based sensor towards O_2 and CO at an applied DC bias of 1 V at 800 ^oC. (D) Real-time selectivity study on impedancemetric Pt-CeO_2 NFs based sensor towards O_2 and CO, operating at 100 kHz with amplitude of 0.5 V at 800 ^oC. Reprinted with permission from Ref. [164].

Figure 1

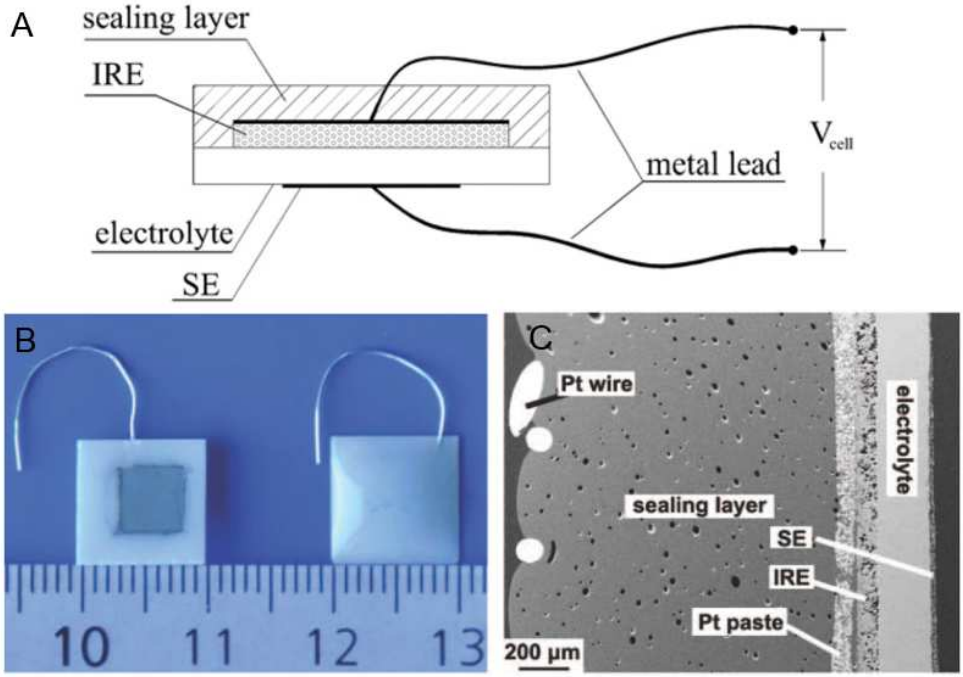

Figure 2

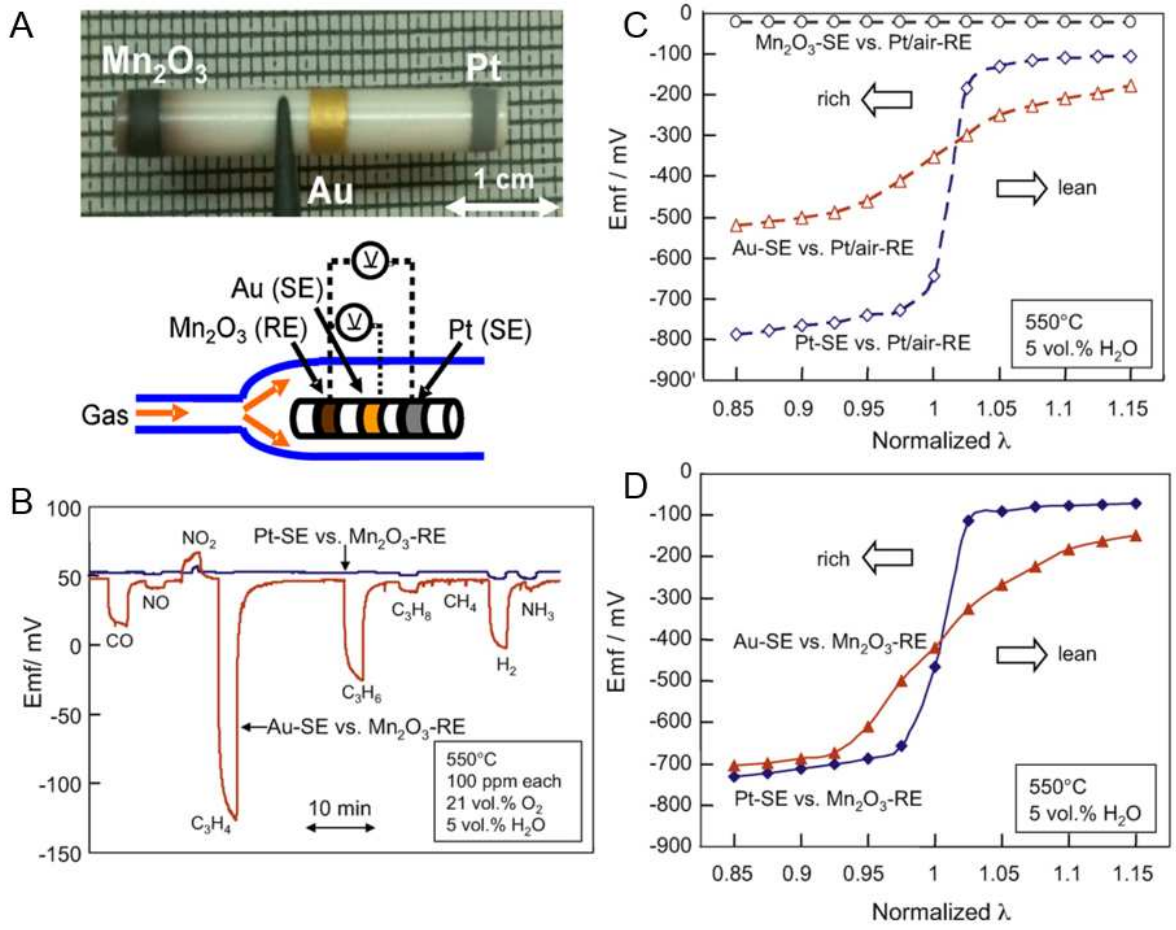

Figure 3

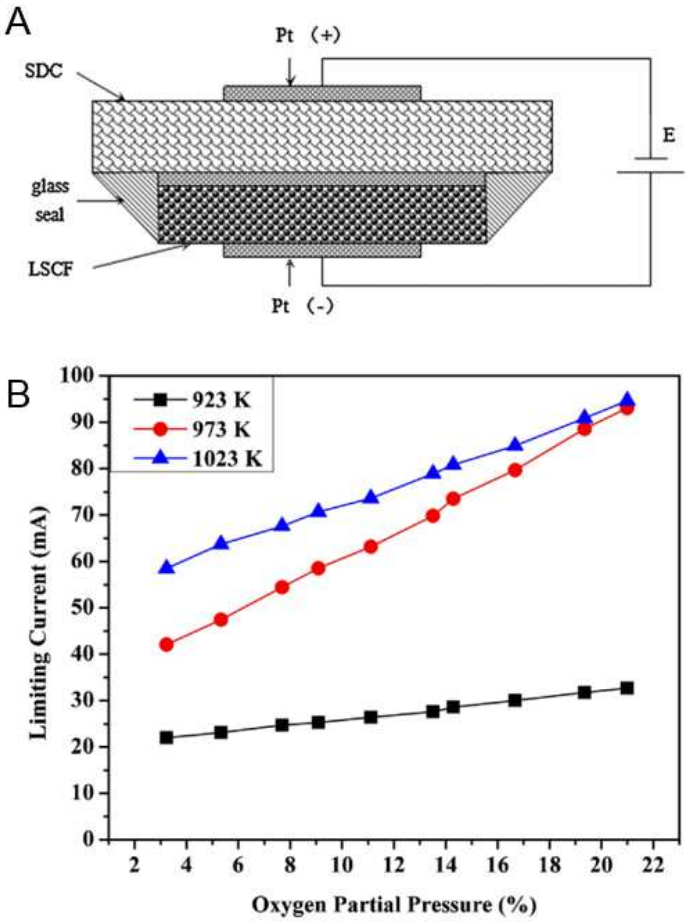

Figure 4

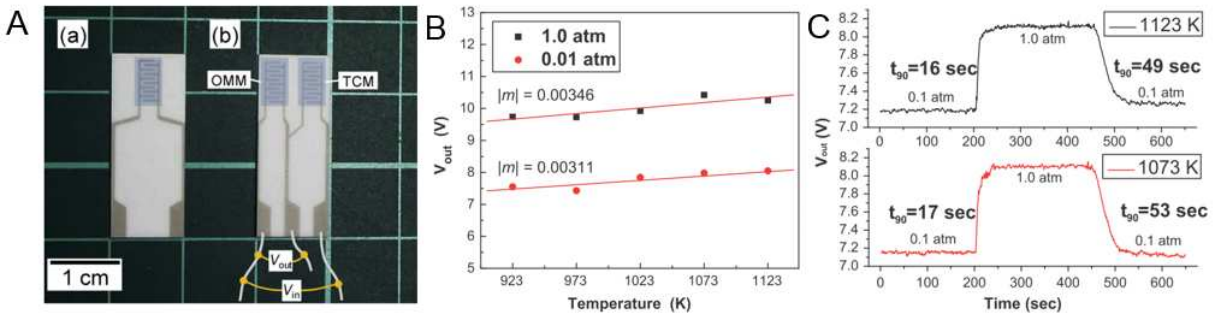

Figure 5

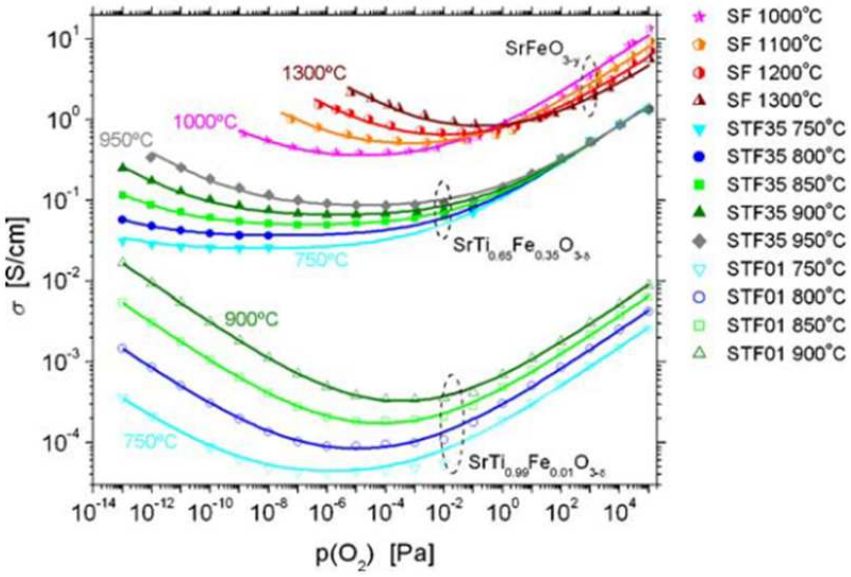

Figure 6

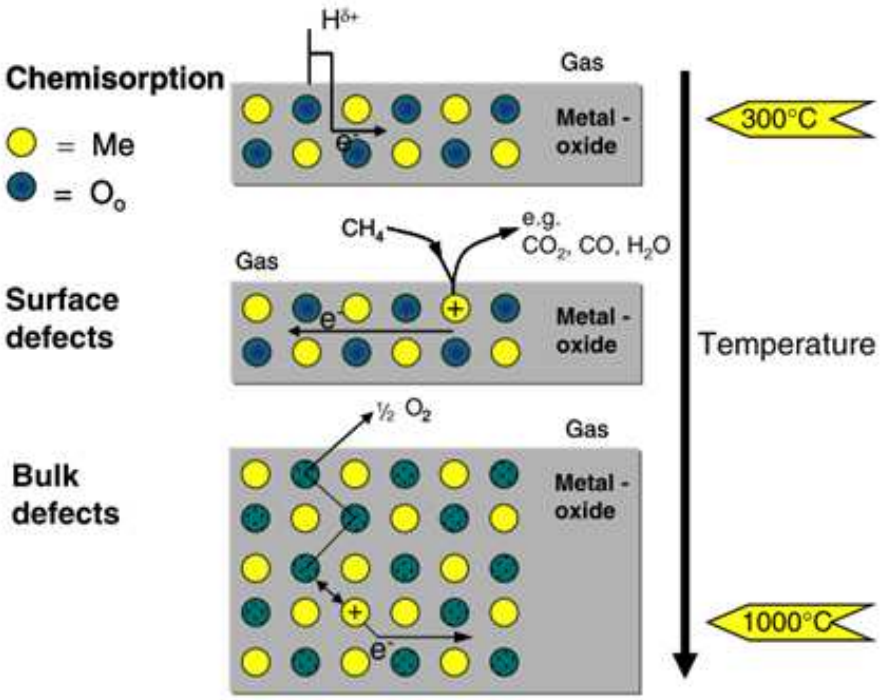

Figure 7

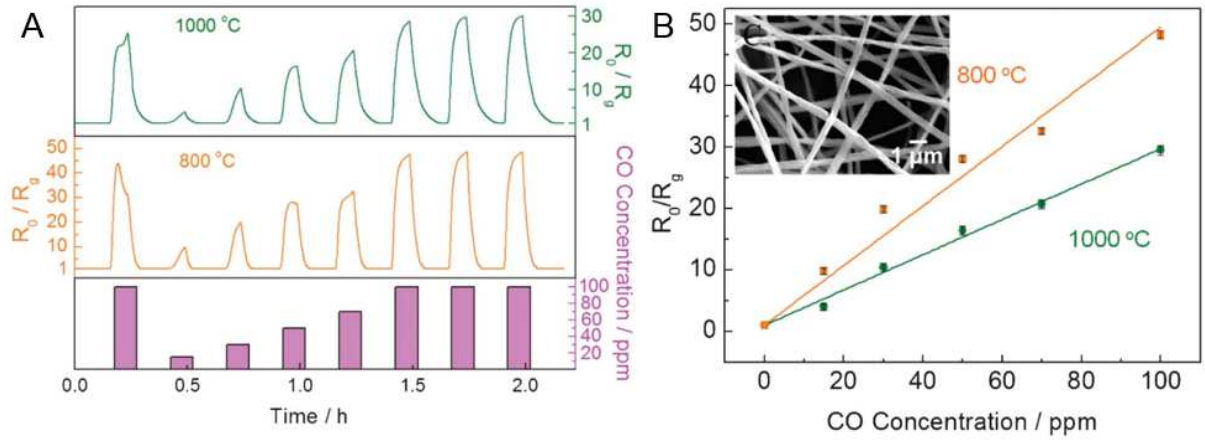

Figure 8

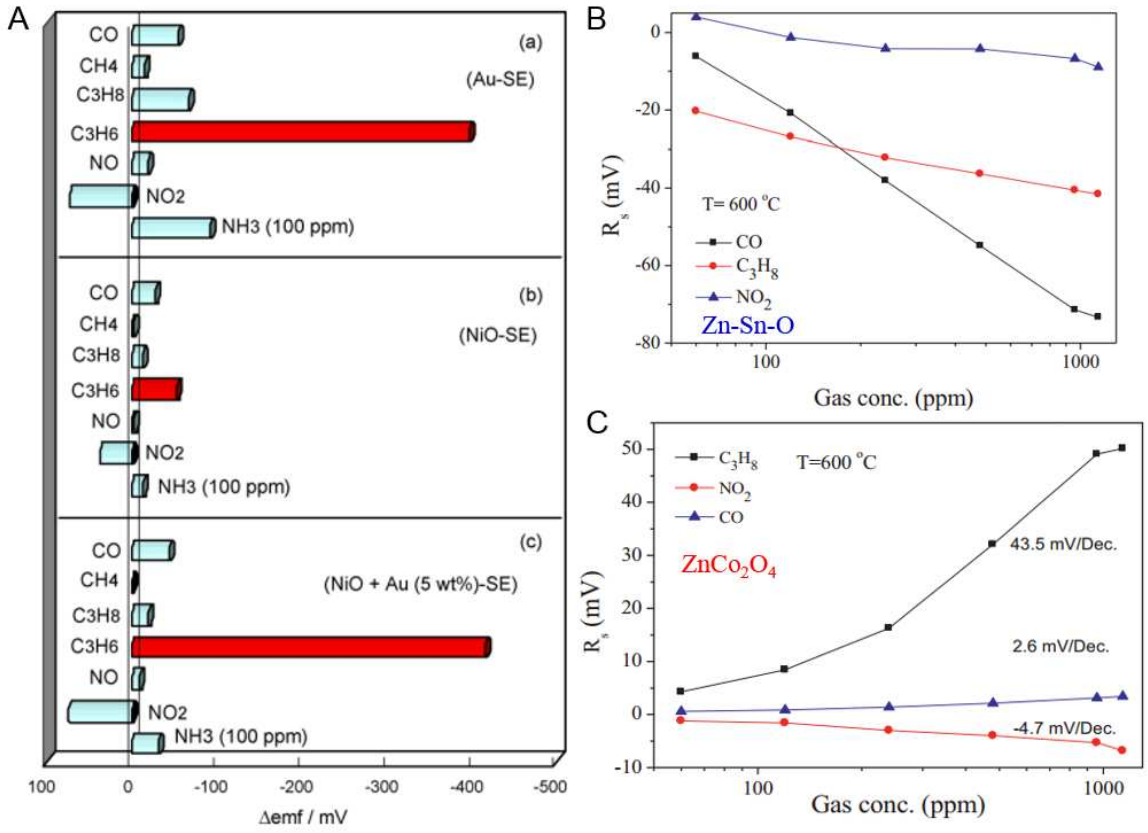

Figure 9

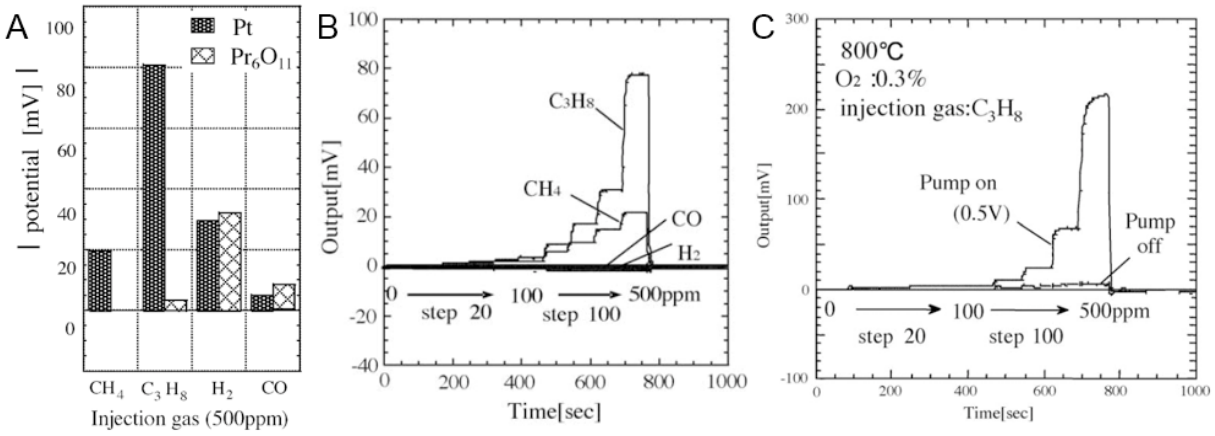

Figure 10

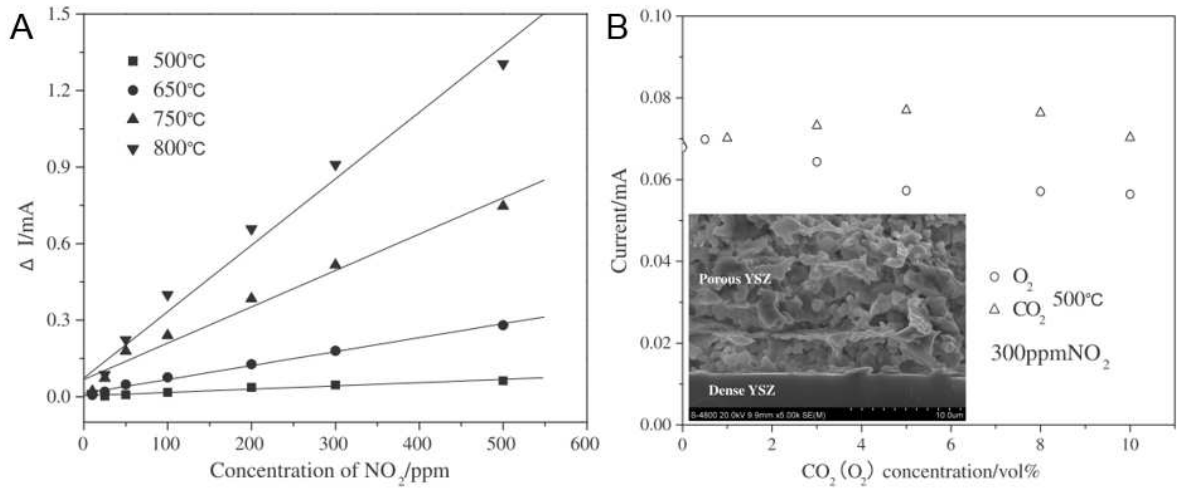

Figure 11

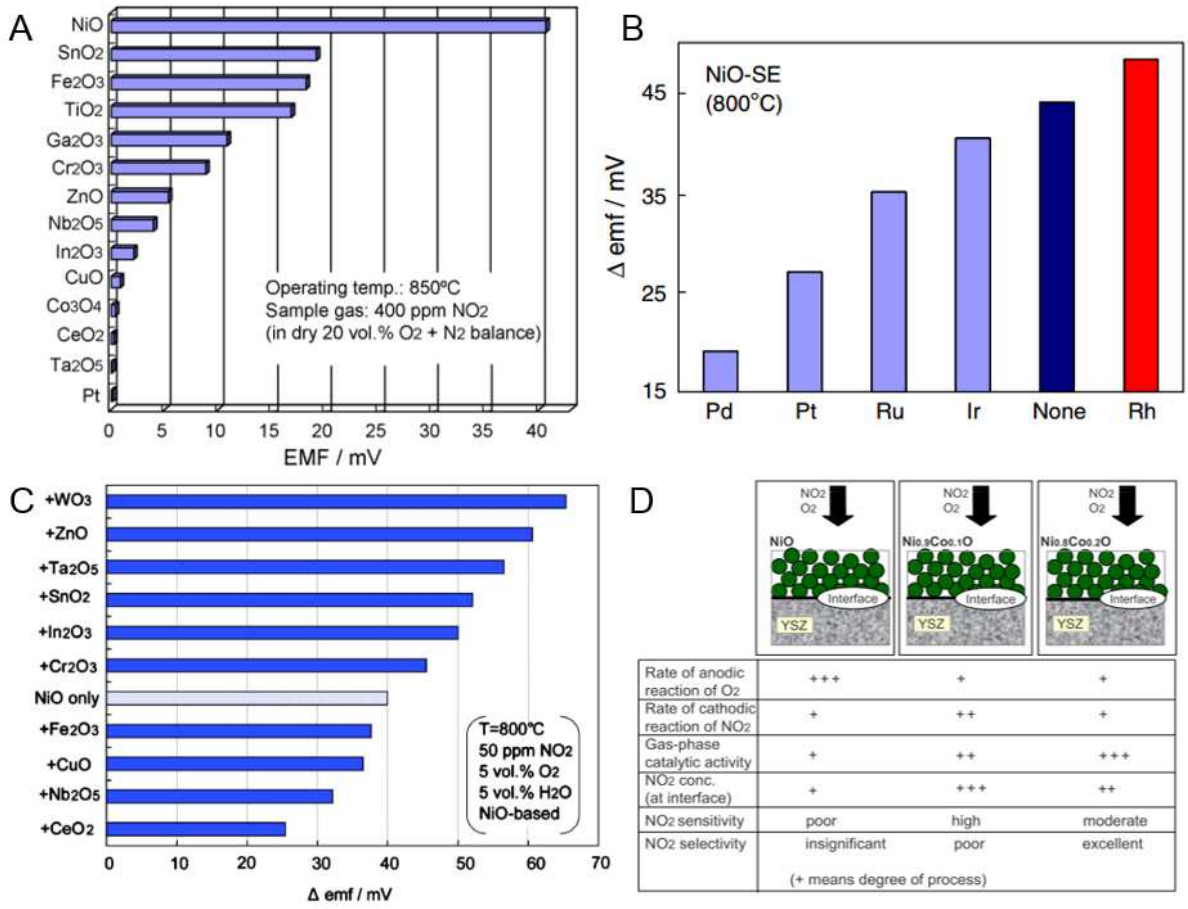

Rate of anodic reaction of O_2	+++	+	+
Rate of cathodic reaction of NO_2	+	++	+
Gas-phase catalytic activity	+	++	+++
NO_2 conc. (at interface)	+	+++	++
NO_2 sensitivity	poor	high	moderate
NO_2 selectivity	insignificant	poor	excellent

(+ means degree of process)

Figure 12

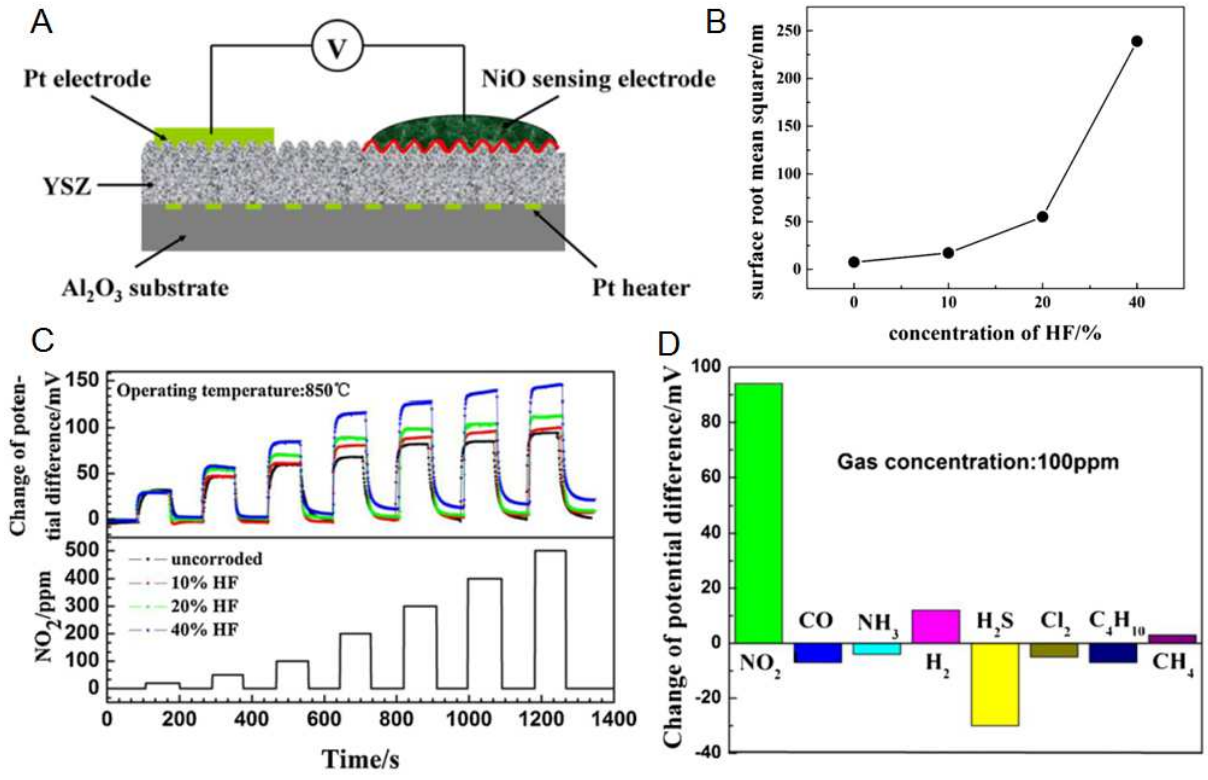

Figure 13

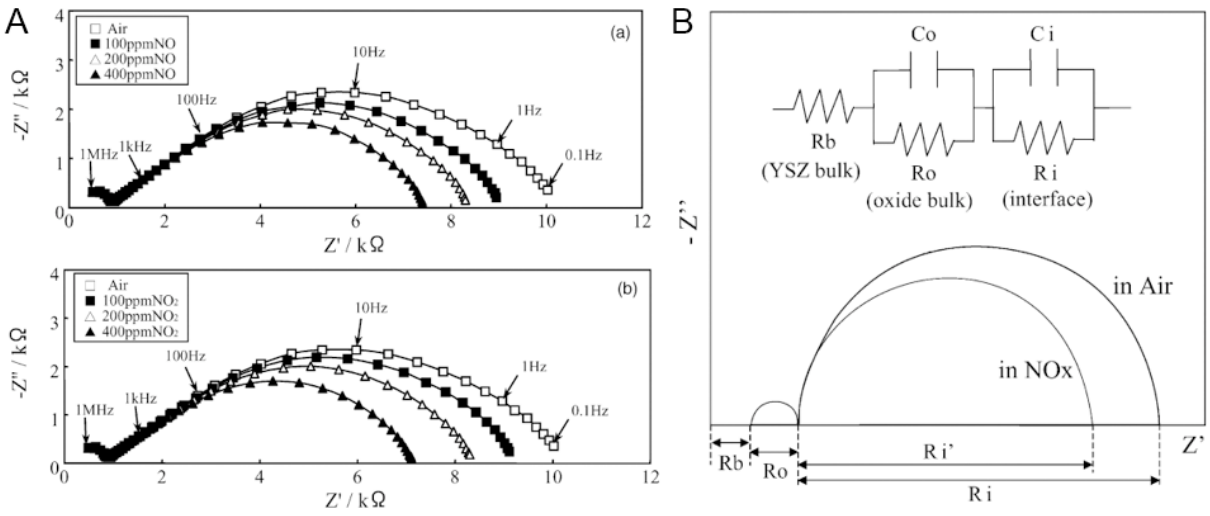

Figure 14

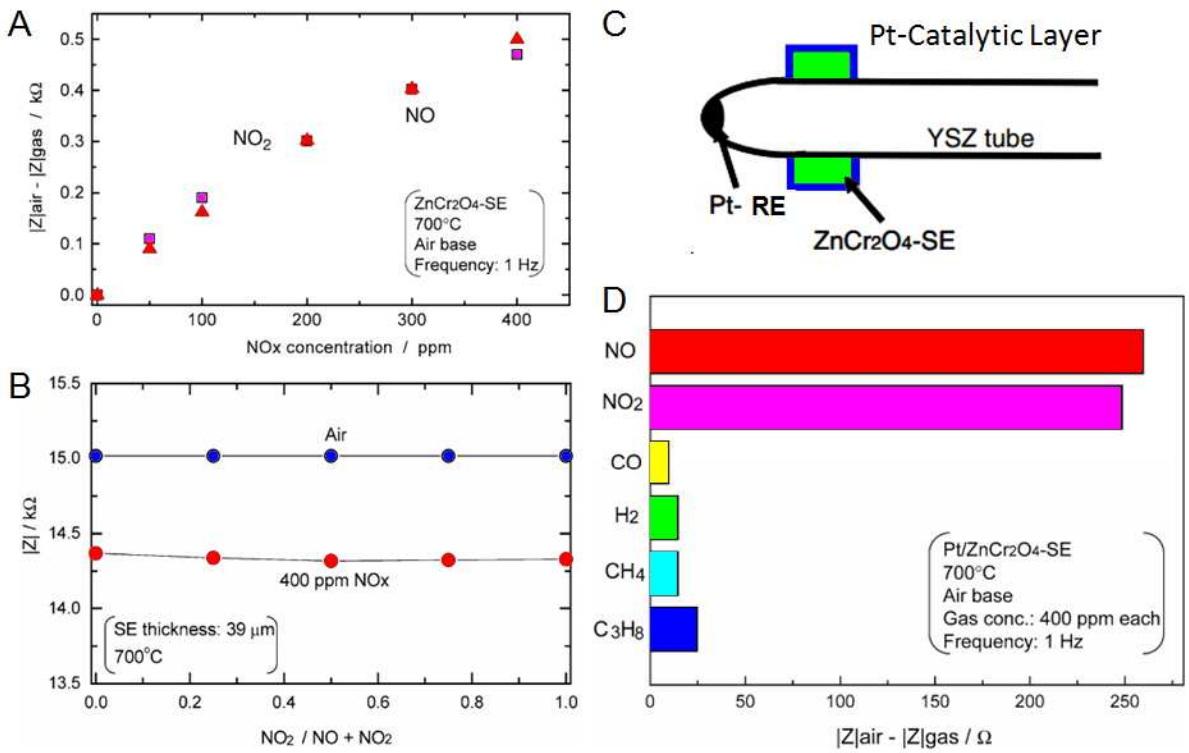

Figure 15

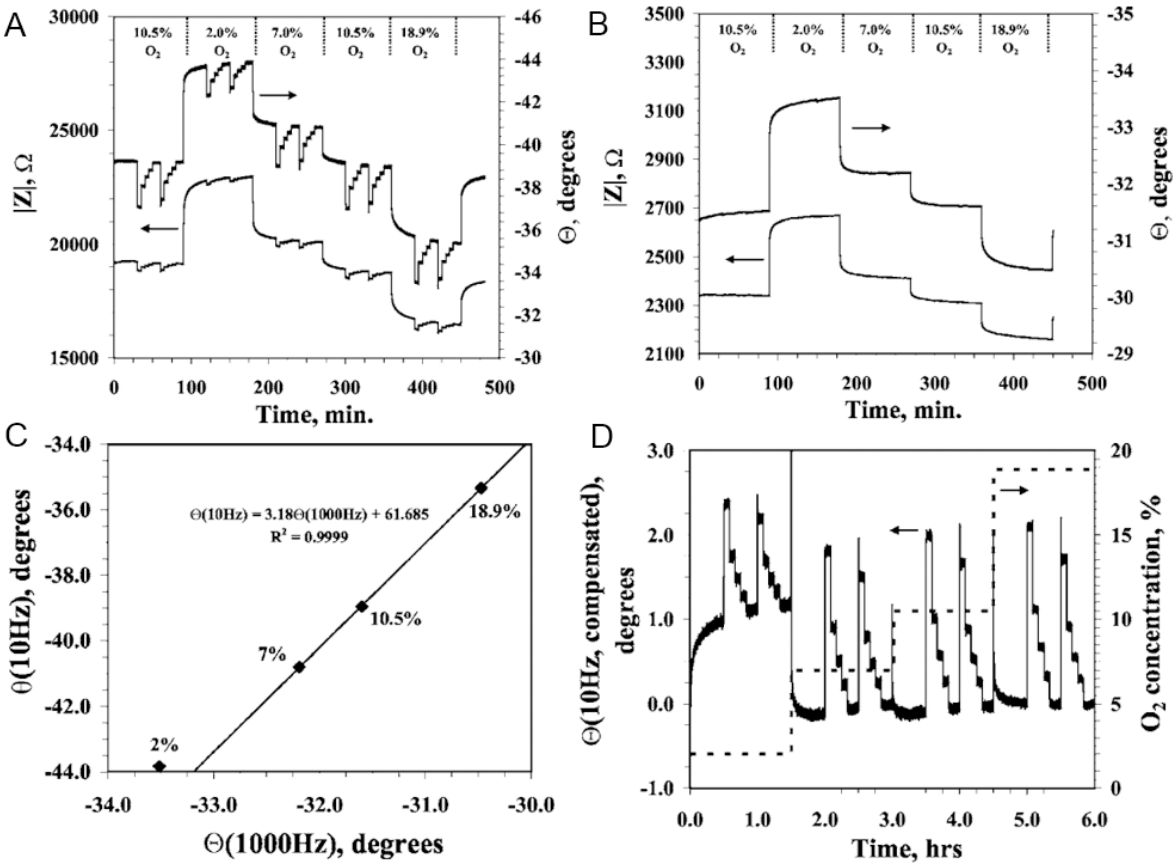

Figure 16

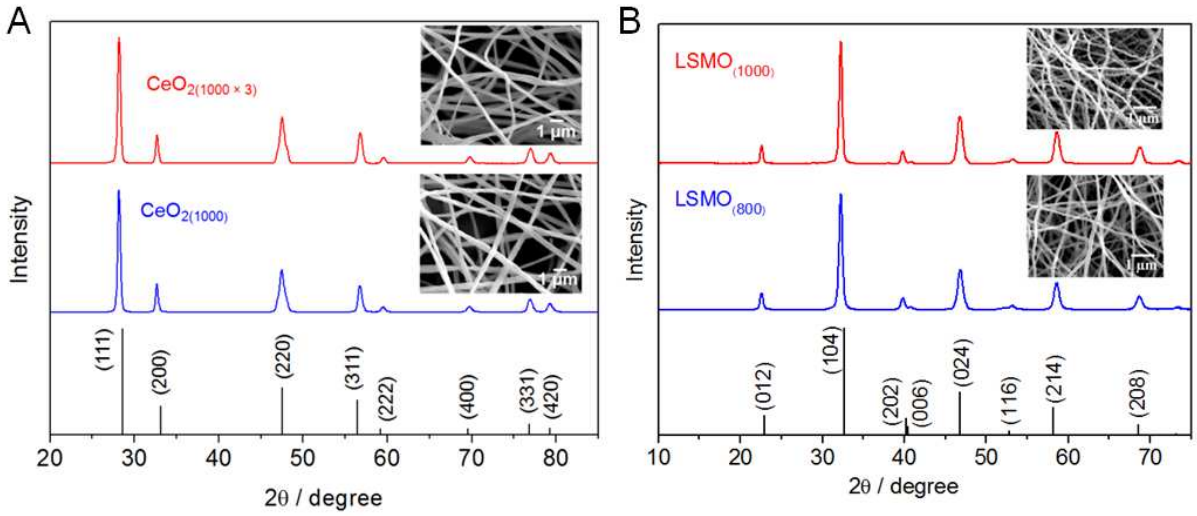

Figure 17

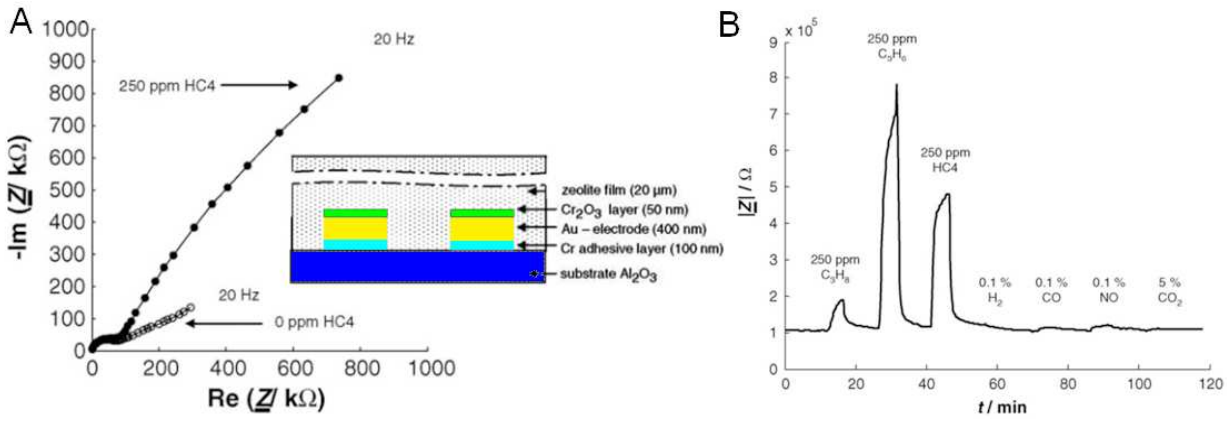

Figure 18

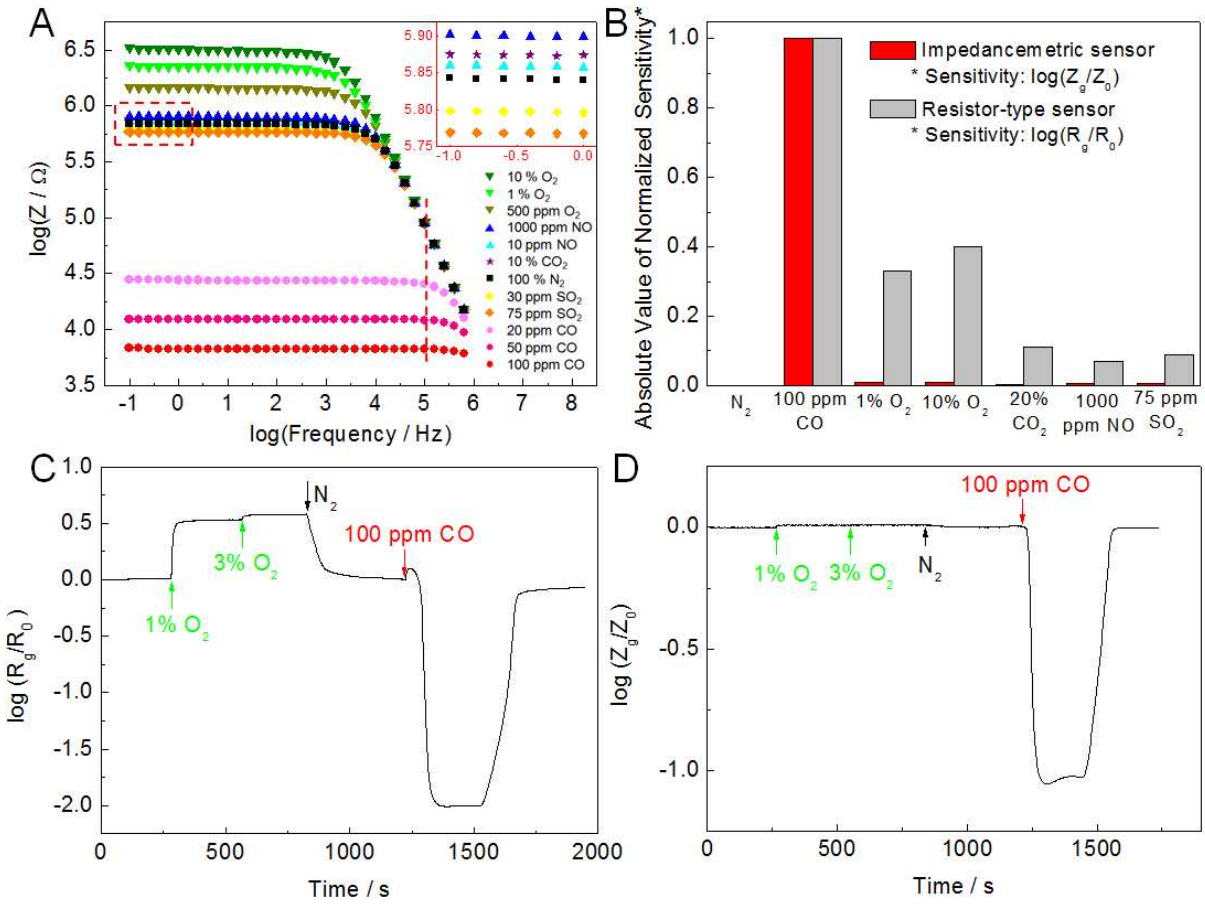

Table 1. Example of exhaust conditions for two- and four-stroke, diesel and lean-four-stroke engines. Reprint with permission from reference [4]

Exhaust components and conditions [a]	**Diesel engine**	**Four-stroke spark ignited-engine**	**Four-stroke lean-burn spark ignited-engine**	**Two-stroke spark ignited-engine**
NO_x / ppm	350–1000	100–4000	≈ 1200	100–200
HC / ppm C	50–330	500–5000	≈ 1300	20,000–30,000
CO	300–1200 ppm	0.1–6%	≈ 1300 ppm	1–3%
O_2	10–15%	0.2–2%	4–12%	0.2–2%
H_2O	1.4–7%	10–12%	12%	10–12%
CO_2	7%	10–13.5%	11%	10–13%
SO_x / ppm	10–100	15–60	20	≈ 20
PM	65 mg/m^3			
Temperatures / ^oC	r.t.–650 (r.t.–420)	r.t.–1100 [b]	r.t.–850	r.t.–1000
λ (A/F) [c]	≈ 1.8 (26)	≈ 1 (14.7)	≈ 1.16 (17)	≈ 1 (14.7)

a. N_2 is remainder. b. Close-coupled catalyst.
c. λ defined as ratio of actual A/F to stoichiometric A/F, λ = 1 at stoichiometry (A/F = 14 . 7).

Table 2. Sensing performance of various resistor-type high temperature (>600 ^{o}C) oxygen sensors

Sensing Material	Operating temperature	Range of detection limits	Response time	Reference
CeO_2	700-1100	-	5-10 ms	166
CeO_2	600-700	$10^3 – 10^5$ Pa	5-10 ms	167
CeO_2 (Pt)	615-1000	$10^3 – 10^5$ Pa	5-11 s	168
CeO_2	800, 1000	0-1%	< 30 s	85
CeO_2 on TiO_2	700	-	-	169
$Ce_{1-x}Zr_xO_2$	600-800	$10^{-17} – 10^5$ Pa	1-20 ms	59
β-Ga_2O_3	480-820	7×10^{-5} Pa	-	170
β-Ga_2O_3	1000	0-100 %	10 s	57
Ga_2O_3(ZrO_2, TiO_2, MgO)	900-1200	0.002 – 0.2 bar	~ 2min	171
Ga_2O_3 (CeO_2, Mn_2O_3, La_2O_3)	500-900	1-20%	~ 2 min	172
$La_{1-x}Sr_xMnO_3$	800	0-1%	< 1 min	160
Nb_2O_5 (TiO_2)	550-750	0.01-100 kPa	~ 5 min	173
TiO_2	600-1000	$10^{-21} – 10^3$ atm	-	56
TiO_{2-x}	200-800	0-100%	-	174
TiO_2 (Cr)	600-800	400-1200 ppm	-	175
$SrTi_{1-y}Nb_yO_3$	800 - 1000	$10^{-13} – 10^5$ Pa	5 – 10 s	176
$SrTiO_3$	750-950	$10^{-13} – 10^5$ Pa	< 30 s	62

Table 3. Sensing performance of resistive sensors towards (>600 ^{o}C) CO and HCs sensors

Material	**Sensing gas**	**Carrying gas**	**Operating temperature/^{o}C**	**Range of detection limits**	**Reference**
$BaSnO_3$	CO	Dry 20% O_2	550-950	0 - 5 vol. %	177
Ga_2O_3 (SnO_2)	CO, CH_4 Iso-Butane	Wet air	500 - 950	1% 100 ppm	82
Ga_2O_3 (Au)	CO	Wet air	500-700	200-5000 ppm	83
Ga_2O_3 (with Rh, Ru, Ir)	Ethanol Propane	Wet air	540-800	25-50 ppm	84
TiO_2 (La_2O_3, CuO)	CO	N_2 (~1ppm O_2)	600	0-1500 ppm	86
TiO_2 (La_2O_3, CuO)	CO	5% O_2	600	0-1000 ppm	87
p-n TiO_2	CO	5% O_2	600	0-1000 ppm	88
TiO_2 (Pt, Cr)	CO	5% O_2	500 - 1000	0-1500 ppm	89
Pt-Zeolite-TiO_2	C_3H_8, CO	5% O_2	600	250-1000 ppm	90
CeO_2	CO	N_2	800, 1000	100 – 800 ppm	85

Table 4. Sensing performance of mixed potential CO and HCs sensors (>600 ^{o}C)

Sensing Cell*	Sensing Gas	Carrying Gas	Operating T/^{o}C	Range of detection limits / ppm	Sensitivity mV·decade^{-1} (T/^{o}C)	Reference
Pt/YSZ/Pt/WO_3	CO	air	500-700	300-1000	-15 (600), -7 (650)	96
Pt/YSZ/Pt/WO_3	CO	air	500-650	200-1000	-27.58 (600), -6.14 (650)	95
Pt/YSZ/Pt/WO_3	CO	air	450-700	20 - 1000	-19.4 (600)	20
Pt/YSZ/Au/Nb_2O_5	CO	air	450-650	200-1000	-29 (600)	19
Pt/YSZ/ Nb_2O_5	C_3H_6	air	550-700	200-1000	-115 (700)	97
Pt/YSZ/ Nb_2O_5:Ta_2O_5 (1:1)	C_3H_6	air	550-700	200-1000	-152 (700)	99
Pt/ScSZ/ITO	CO	air	615	100-400	87.1	104
Au/YSZ/$LaCoO_3$/Au	CO, C_3H_6, C_3H_8	O_2 contenting	600, 700	0-4000	-	106
Au/$LaMnO_3$/YSZ/TbYSZ/Au	CO, C_3H_6, C_3H_8	1.74% O_2	600, 700	0 – 500	-	107
Pt/YSZ/CdO	C_3H_6	air	600	20-1000	Cal. 75	109
Pt/YSZ/NiO(Au 5%)	C_3H_6	5 vol% H_2O 5 vol% O_2	600	10-400	Cal. 230	110
Pt/YSZ/Au-Ga_2O_3	C_3H_6	1.5% O_2	700	0-8000	-	178
Au/YSZ/Au/Ta-doped TiO_2	C_3H_6, C_3H_8	air	450–650	200-1000	-5.5 (600 ^{o}C)	179
Pr_6O_{11}/YSZ/Pt	CH_4, C_3H_8	0.2–0.3% O_2	800	0-500	-	112
Pt/YSZ/Zn_2SnO_4+SnO_2	CO	20% O_2	600	60-1500	-56.65	111
Pt/YSZ/$ZnCO_2O_4$	C_3H_8	20% O_2	600	60-1500	43.5	111

*RE/electrolyte/SE

Table 4. Sensing performance of mixed potential NO_x sensors (>600 ^oC)

Sensing Cell	Sensing Gas	Carrying Gas	Operating T/^oC	Range of detection limits / ppm	Sensitivity mV·decade^{-1} (T/^oC)	Reference
Pt/YSZ/Pt/WO_3	NO_2	air	500-700	300-1000	18.8 (600), 13.14 (700)	96
Pt/YSZ/Pt/WO_3	NO_2	air	500-650	200-1000	12.54 (600), 6.68 (650)	95
Pt/YSZ/Pt/WO_3	NO_2	air	450-700	20 - 1000	17.8 (600), 7.5 (700)	20
Pt/YSZ/$NiCr_2O_4$	NO_2, NO	air	550 -650	25 - 436	Cal. 63(NO_2), -25(NO) (650)	128
Pt/YSZ/$ZnFe_2O_4$	NO_2, NO	air	600 - 700	50 - 436	Cal. 32(NO_2), -7(NO) (700)	129
Pt/YSZ/$ZnCr_2O_4$	NO_2, NO	air	600 - 700	50 - 436	Cal. 10(NO_2), -4(NO) (700)	130
Pt/YSZ/ $ZnFe_2O_4$-$ZnCr_2O_4$	NO_2	air	600 - 700	50 - 436	Cal. 60 (700)	130
Pt/YSZ/ZnO	NO_2, NO	air	600-700	40-450	Cal. 45(NO_2), -17(NO) (700)	132
Pt/YSZ/Pt/$LaFeO_3$	NO_2	air	450-700	20–1000	-11 (600), -3.7 (650)	20
Pt/YSZ/Pt/$La_{0.8}Sr_{0.2}FeO_3$	NO_2	air	450-700	20–1000	-13.6 (600)	20
Pt/YSZ/NiO (1300 ^oC sintered)	NO_2	wet gas*	800 - 900	50–400	Cal. 28 (900)	136
Pt/YSZ/NiO (1400 ^oC sintered)	NO_2	wet gas	800 - 900	10–400	Wet: Cal. 48 (850), 45 (900) Dry: Cal. 39 (850), 33 (900)	135
Pt/YSZ/NiO (thin film)	NO_2	wet gas	600–800	50–400	Cal. 12 (800)	137
Pt/YSZ/NiO (modified TPB)	NO_2	air	850	20-500	Cal. 75	147
Pt/YSZ/NiO-CuO(10%)	NO_2	wet gas	800	50–400	Cal. 19	141
Pt/YSZ/NiO-WO_3(10%)	NO_2	wet gas	800	50-400	Cal. 50	142
Pt/YSZ/NiO-WO_3/Cr_2O_3	NO_2	wet gas	700-900	50-400	Cal. 35 (895)	143
Pt/YSZ/NiO-Rh(3%)	NO_2	wet gas	800-850	5-100	Cal. 62 (800), 60 (850)	140
Pt/YSZ/Cr_2O_3-WO_3	NO_2, NO	air	800	2-300	Cal. 25(NO_2), -3.2(NO)	180
Pt/YSZ/$Ni_{0.95}Cr_{0.03}O_{1-\delta}$	NO_2	wet gas	800-900	50-400	Cal. 45(800), 36 (900)	144
Pt/YSZ/$Ni_{0.9}Co_{0.1}O_3$	NO_2	wet gas	800	50-400	Cal. 41	145
Pt/YSZ/$MnCr_2O_4$	NO_2	air	800	10-500	Cal. 36	148

*5 vol.% O_2 + 5vol.% H_2O Cal: sensitivity is proximately calculated on reported calibration curve.

Table 5. Sensing performance of impedancemetric NO_x sensors (>600 ^oC)

Sensing electrode	Sensing gas	Carrying gas	Operating T/^oC	Range of detection limits / ppm	Reference
Pt/YSZ/$ZnCr_2O_3$	NO, NO_2	air	600-700	50-400	28, 150
Pt/YSZ/$ZnCr_2O_4$	NO_2	air	700	0-400	131
Cr_2O_3/YSZ/Cr_2O_3	NO, NO_2	O_2 containing	600	8-50	151
$LaMnO_3$/YSZ/ $LaMnO_3$	NO, NO_2	10.5% O_2	550-650	0-100	27
Au/YSZ/Au	NO, NO_2	2% O_2	600-700	10 -100	34
Porous Pt/YSZ/Au	NO, NO_2	10% O_2	650	0-100	153
Pt/YSZ/Au	NO, NO_2	10.5% O_2	650-670	25-250	158
Me/YSZ/Me (Me=Au, Ag, or Pt)	NO, NO_2	O_2 containing	600-700	100	152
Pt/YSZ/NiO NPs	NO_2	N_2 or 5% O_2	600	0-300	154
Pt/YSZ/$NiCr_2O_4$	NO	N_2 or 5% O_2	500-700	50 – 950	155
Au/YSZ/$LaCr_{0.95}Mg_{0.05}O_3$	NO, NO_2	O_2 containing	600-700	10-50	156

Biographies

Yixin Liu is a Ph.D. student in the Department of Chemical and Biomolecular Engineering, University of Connecticut, USA. She earned her Bachelor degree in 2010 from Zhejiang University, China. Her research concentrates on functional nanomaterial for chemical sensing including harsh environmental sensing.

Joseph Parisi is a Ph.D. student in the Department of Chemical and Biomolecular Engineering, University of Connecticut, USA. His research concentrates on microfluidic based chemical and biological sensing.

Xiangcheng Sun is a Ph.D. student in the Department of Chemical and Biomolecular Engineering, University of Connecticut, USA. He earned his Bachelor and Master degree from Harbin Institute of Technology-China and Chinese Academy of Sciences in 2008 and 2011, respectively. He has expertise in the design, development and validation of various electrical and optical sensors for various targets.

Yu Lei is a Castleman associate professor of Chemical and Biomolecular Engineering at the University of Connecticut, USA. Dr. Lei obtained his Ph.D. degree in 2004 at the University of California-Riverside in Chemical and Environmental Engineering. His current research combines biotechnology, nanotechnology, and sensing technology, especially as applied to the development of gas sensors, electrochemical sensors, and biosensors.